Towards Intuitive Control of Simultaneous Movements and Force Estimation for Myoelectric Prostheses

Group 1072 | Master Thesis | Spring 2012
Jakob Celander Rosenvang & Ronnie Horup
Supervisor: Ernest Nlandu Kamavuako & Winnie Jensen

Aalborg University | Biomedical Engineering and Informatics

AALBORG UNIVERSITY

Department of Health Science and Technology
Aalborg University
Fredrik Bajers Vej 7 D2
Phone +45 99 40 99 40
Fax +45 98 15 40 08
http://www.hst.aau.dk/

Title:

Towards Intuitive Control of Simultaneous Movements and Force Estimation for Myoelectric Prostheses

Project period:

4th Semester, Spring, 2012

Master Thesis

Project group:

Medical Systems - 1072

Participants:

Jakob Celander Rosenvang

Ronnie Horup

Supervisors:

Ernest Nlandu Kamavuako
Winnie Jensen

Copies: 5
Pages: 92
Finished: June 1st, 2012

Many people live with a hand amputation, which greatly impacts the quality of their life. However, some functionality can be regained using a myoelectric hand prosthesis. Currently, many advances have been made towards recovering as many functionalities of the hand as possible including several sequential movements. However, to make control of myoelectric prosthesis more intuitive and less robot like, still lacking is a control system allowing precise control of simultaneous movements and the corresponding force.
To develop such a control system, an experiment was conducted including 10 healthy subjects. The data acquired through the experiment was used to develop a control system allowing 8 distinct wrist movements at continuous force levels along with rest. The control system was optimized through an investigation of parameters affecting the performance of the system.
Validation showed that such a system could be developed, resulting in a classification accuracy of 92.2 % for nine movements. Furthermore, the corresponding force could be precisely estimated with an R^2 of 0.92.
We have developed a novel hybrid control scheme capable of simultaneous control of two DoFs achieving high accuracies for both movement classification and force estimation, which is suitable for real-time control.

Preface and reading guide

Preface

This project was made by group 1072 as part of the 10th semester at the master specialization in Medical Systems at Biomedical Engineering & Informatics at Aalborg University. The project was conducted in the period February 1st to June 1st 2012. This report focuses on the development of a control system allowing control of multiple simultaneous DoFs along with the corresponding force for a myoelectric prosthetic device.

The project is aimed at fellow students and others with interest in the topics investigated. However, the proposed control system is targeted to the research field of myoelectric prosthesis and control of these.

Reading guide

In the introduction to this report the focus is outlined. Following, the report is divided into three parts. In the first part called *Analysis* the focus is investigated and the final problem statement is introduced. The second part, *Experiment*, investigates and answers the initial problem statement leading to the third part, *Synthesis*, where the results are discussed and a conclusion is made.

References are made according to the Harvard method, where authors' last name and the year of publication are placed in brackets as so, [Last name, Year]. If references are given for a specific sentence, the reference is found within the sentence, while it is placed right after the punctuation if the reference is given for the entire previous paragraph. All references used can be found in *Bibliography*, listed in alphabetical order.

Tables and figures throughout the report are numbered according to the chapter they appear in (figure 1 in chapter 2 is numbered as figure 2.1). Both tables and figures include a caption and a reference to the source if any. Figures and tables with no reference are made by the authors of the report.

Contents

1 Introduction **1**

I Analysis **5**

2 Effect of an amputation on the anatomy of the lower arm **7**
2.1 Muscles of the forearm and the corresponding movements 7
2.2 Diversity of muscle location due to amputation 9

3 EMG response during muscle activation **11**
3.1 Neural control of skeletal muscles 11
3.2 Voluntary contraction of a skeletal muscle 11
3.3 Measurement of myoelectric signals 13

4 Myoelectric control schemes **15**
4.1 State control 16
4.2 Pattern recognition 16
4.3 Proportional control 21
4.4 Pros and cons of myoelectric control schemes 22

5 Aim **25**

II Experiment **29**

6 Experimental design **31**
6.1 Subjects 31
6.2 Degrees of Freedom 31
6.3 EMG acquisition 32
6.4 Force profiles for execution of movements 33
6.5 Setup 35
6.6 Procedure 37

7 Data Processing **39**
7.1 Filters 39
7.2 Features 39
7.3 Dimensionality Reduction 45

7.4 Classification 46
7.5 Force estimation 52
7.6 Statistical analysis 53

8 Optimization and validation strategy **55**
8.1 Optimization of parameters 55
8.2 Validation of system 58

9 Results **61**
9.1 Effect of different combinations of TD features 61
9.2 Effect of different feature domains 62
9.3 Effect of different windows 63
9.4 Effect of filtering features 63
9.5 Effect of classifier and dimensionality reduction method 64
9.6 Effect of post-processing 66
9.7 Effect of force estimator 67
9.8 Validation of control system 68
9.9 Summary of results 72

III Synthesis **75**

10 Discussion **77**

11 Conclusion **83**

12 List of abbreviations **85**

Introduction

1

The loss of a limb due to an amputation greatly reduces the quality of life (QoL) for the affected person. Especially the loss of the hand impacts the QoL due to its frequent use for grasping and moving small and large objects. In the USA an estimated 1.2 to 1.9 million people live with an amputation (excluding loss of a toe or fingertip) with 185.000 new cases each year. The main reasons for an amputation are congenital, surgery, trauma, or as a consequence of disease such as diabetes. [Winkler, 2009; Epstein et al., 2010; Esquenazi, 2004]

QoL may be increased for persons with hand amputation by use of a hand prosthesis, which helps to recover some of the lost functionality of the hand. Types of prosthetic devices range from passive cosmetic prostheses, that assist amputees to regain a near-normal look, to active prostheses regaining some functionality. Active prostheses are either body-powered or electrical. Especially myoelectric prostheses (controlled based on muscle signals) are useful in recovering multiple hand movements while maintaining a near-normal cosmetic look. However, as the hand is very complex, it is currently impossible to regain all its functionality (both motor and sensor functions). [Epstein et al., 2010; Miguelez et al., 2010; Cotton et al., 2007] Myoelectric prostheses utilizes information encoded in the electromyogram (EMG) arising from muscle contractions of the residual limb. This information is decoded to create a control signal for the prosthetic device, which performs the intended movement. A schematic representation of such a system can be seen in figure 1.1, where the control system extracting the information and generating control signals for the prosthesis is regarded as a black box. [Parker et al., 2006]

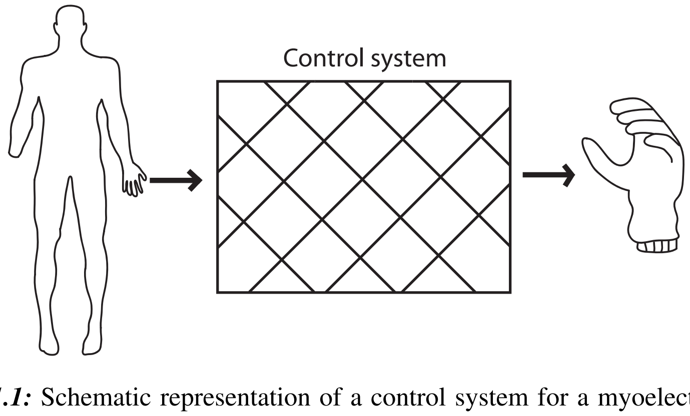

Figure 1.1: Schematic representation of a control system for a myoelectric prosthesis.

The focus of this project is on persons with transradial (below elbow) amputation, since amputation at higher levels (above elbow) causes all intrinsic and extrinsic muscles of the hand and wrist to be lost, consequently making direct myoelectric control very difficult.

Current commercially available myoelectric prostheses only implement a very limited amount of movements with only one movement at a time, e.g. grasping. Control is not always intuitive and can require long training periods. [Cotton et al., 2007; Parker et al., 2006]

Current research has mainly followed two paths in trying to improve control of prosthetic devices: 1) Improving the number and the robustness of controllable movements, and 2) allowing prosthetic devices to be activated at different force levels. Both functionalities are important to regain, as these would allow the amputee to perform many movements and to adjust the force of the movements. This would enable the amputee to e.g. grasp a bottle of water with enough force to hold it without squeezing it.

Currently, many researches have proposed control systems, which allow accurate control of multiple, sequential movements; for example, by Scheme et al. where 11 sequentially controllable movements (4 movements of the wrist/forearm, five different grips and no movement) could be controlled with high accuracy. Although less investigated, a relation between force and myoelectric signals has been established for both sequential and combined movements; for example by Nielsen et al. where the intended force of two movements and a combination of these was estimated with high precision. Although these results are promising, there are still many challenges towards recovering more functionalities for amputees. [Scheme et al., 2011; Nielsen et al., 2011]

The ultimate goal for control of a prosthetic hand, as stated by Parker et al., is:

"The ultimate goal of this development work is to have simultaneous, independent, and proportional control of multiple degrees of freedom with acceptable performance (classification rate and active daily living) and near 'normal' control complexity and response time."

To approach this goal, it is necessary to combine the two paths to achieve several controllable movements while at the same time allowing different forces to be exerted. Furthermore, such a system must be able to control more than one movement simultaneously (i.e. simultaneously control multiple degrees of freedom) while keeping the control of the system as simple as possible for the user. This leads to the initial problem statement:

Initial problem statement

How can the control of myoelectric prosthesis be improved to allow both simultaneous movements and precise control of the corresponding force?

In order to answer the initial problem statement, it was necessary to investigate the components of the control system, see figure 1.1. In general, myoelectric control of a prosthesis typically involves an investigation of the following three steps [Parker et al., 2006]:

1) Locating a source of myoelectric signals

To locate an appropriate source of myoelectric signals, it is essential to understand the functionality of a healthy hand and the muscles which control it. Furthermore, it is necessary to investigate the differences caused by the amputation.

2) Identifying the information available in the signal

When the signal source has been identified, the myoelectric signal can be measured and used as control input. However, for advanced control of a prosthesis, it is important to identify the type of information concealed within the signal and the different ways to measure the myoelectric signals.

3) Extracting and applying information from the signal for control

The final step is to extract and convert the information in the myoelectric signal to a control signal for the myoelectric prosthesis. This is done by identifying the methods needed to generate the control signal based on the myoelectric signals.

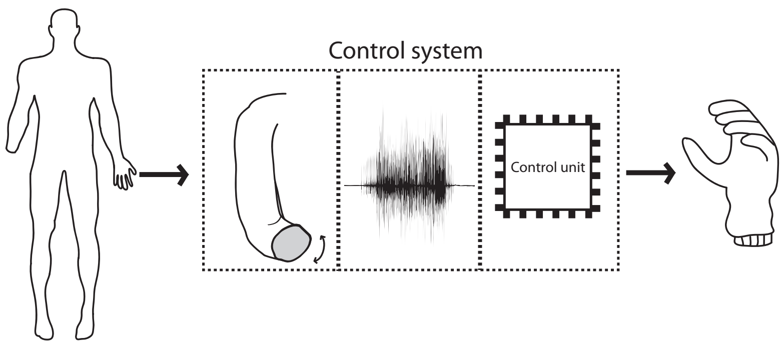

Figure 1.2: Schematic representation of the steps to investigate in myoelectric control system design.

Through these steps, an intended movement can be associated to a performed movement of the prosthesis, as shown in figure 1.2. The analysis will go into each of these steps and thus form a basis for selecting the elements needed for improving the control system and thereby answer the initial problem statement.

Analysis

I

Effect of an amputation on the anatomy of the lower arm 2

In order to utilize myoelectric signals for control of a prosthesis, it is necessary to have knowledge of the underlying anatomy of the muscles. Moreover, it is necessary to understand the coupling between the muscles and movements, and the influence of an amputation.

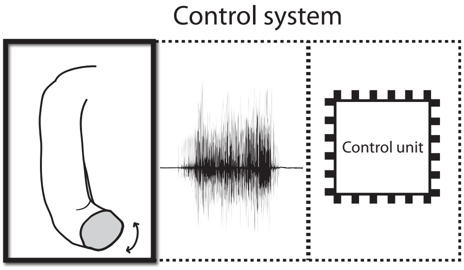

2.1 Muscles of the forearm and the corresponding movements

The hand governs multiple functionalities in daily life, which can be divided into motile and non-motile functions. The non-motile functionality enables sensory feedback of, e.g., the surface texture and the temperature of an object, or the amount of force produced on the object. The motile functionality allows fine and gross motor control of the limb. [Jones and Lederman, 2006]
For control of a myoelectric prosthesis, both the motile and non-motile functionalities are of importance. The non-motile functionalities can be used to e.g. mimic the behavior of mechanoreceptors and thus be used to adjust the grasping strength. The motile functionalities are important to regain motion. These are controlled by 29 different muscles, mostly extrinsic, which altogether allows more than 20 DoFs. [Kendall et al., 2005; Jones and Lederman, 2006]

For a short below-elbow amputee, all intrinsic muscles of the hand are no longer present and thus muscles controlling many DoFs of the fingers are lost and cannot be used for direct, intuitive control of a prosthesis. Therefore, it is unlikely that all DoFs of the fingers can be restored for an amputee. However, the possibility of controlling collective finger flexion and extension directly from extrinsic muscles of the forearm still remains. The muscles of the proximal third of the forearm can be seen on figure 2.1. [Kendall et al., 2005]

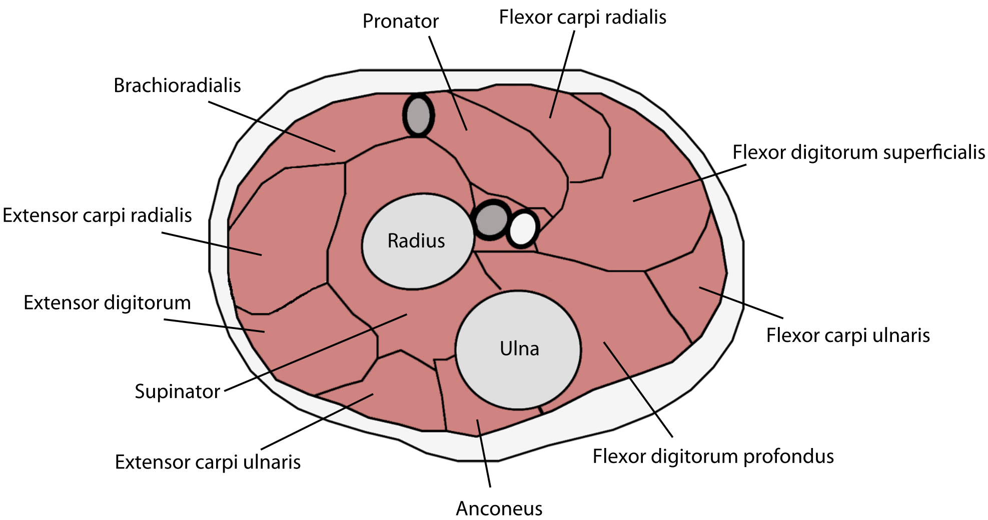

Figure 2.1: Cross sectional view of the proximal third of the forearm.

Still existing are muscles governing the DoFs of the wrist, namely flexion/extension, pronation/supination, and radial/ulnar deviation. All the muscles of the proximal part of the lower forearm and their associated movements are listed in table 2.1. [Kendall et al., 2005; Jones and Lederman, 2006]

	DoF		DoF		DoF		DoF	
	Finger flexion	Finger extension	Wrist flexion	Wrist extension	Radial deviation	Ulnar deviation	Pronation	Supination
Anconeus							X	X
Brachioradialis							X	X
Extensor Carpi Radialis Brevis				X	X			
Extensor Carpi Radialis Longus				X	X			
Extensor Carpi Ulnaris				X		X		
Extensor Digiti Minimi		X						
Extensor Digitorum Communis		X		X	X			
Flexor Carpi Radialis			X		X		X	
Flexor Carpi Ulnaris			X			X		
Flexor Digitorum Superficialis	X		X					
Flexor Digitorum Profundus	X		X					
Palmaris Longus			X					
Pronator Teres							X	
Supinator								X

Table 2.1: Summary of the extrinsic muscles along with their corresponding movements.

Of these movements, ulnar and radial deviation are the least useful in daily life due to the very limited range of motion. However, the three remaining DoFs are all important in everyday life and regaining these would be very beneficial and improve the quality of life for transradial amputees. [Jones and Lederman, 2006]

2.2 Diversity of muscle location due to amputation

Despite whether an amputation is congenital, traumatic or due to surgery, the anatomy of the remaining limb differs greatly from a healthy arm. Apart from congenital amputations, surgery is performed, where several methods are used to improve the outcome. These include beveling the bone, shortening of the nerve as well as performing myoblasty or myodesis (attaching agonist-antagonist muscle pairs or stitching the muscle to the bone, respectively). Performing myoblasty and myodesis allows tension in the muscles, which is necessary in order to use myoelectric prosthesis. [Kelly et al., 2011]
Common for all transradial amputations is the changed anatomy and thus the mapping between the muscle and an intended movement, as described in table 2.1, is changed. Therefore, taking advantage of the associations between muscles and movements might not be beneficial for control of a myoelectric prosthesis.

A study by Farrell and Weir investigated the potential use of untargeted techniques, i.e., recording of unspecified (random) muscles, for control of a myoelectric prosthesis. The results showed that the untargeted technique provided controllability of a prosthesis comparable to that of the targeted technique. These results suggest that intuitive myoelectric control of several movements is feasible in amputees as long as several muscles of the forearm remain. The untargeted technique also makes the job of fitting/designing a prosthesis easier as no specific muscles has to be located. Instead the recording sites can be equally spaced around the forearm [Farrell and Weir, 2008a; Kelly et al., 2011].

EMG response during muscle activation 3

To improve control of a myoelectric prosthesis, it is not only necessary to investigate the anatomy of the lower arm but also the underlying neurophysiology during muscle contraction. In particular the myoelectric signals are of importance, as these are the sources of information for controlling myoelectric devices.

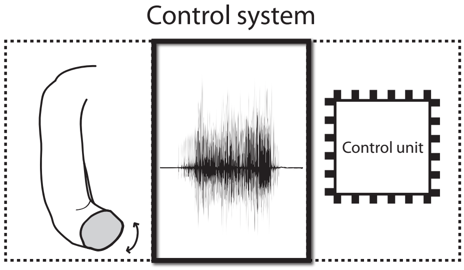

3.1 Neural control of skeletal muscles

The somatic nervous system is the efferent part of the peripheral nervous system associated with voluntary control of skeletal muscles. All voluntary muscular control (except reflexes) emanates from the motor neurons of the central nervous system (CNS) located in the pre- and primary motor cortex. Evoked action potentials originating from this area travels through the corticospinal pathway. For voluntary movement of the upper extremity, the action potentials are conveyed through the corticospinal tracts, which synapse on the lower motor neurons in the anterior gray horns of the spinal cord. Roughly 85 % of these axons decussate in the medulla oblangata, forming the lateral corticospinal tract, and the remaining 15 % form the anterior corticospinal tract. In the latter case, the axons decussate at their level of termination onto the lower motor neuron. In both cases the connection is established through a synapse. The action potentials then reach the lower motor neurons innervating the flexor muscle and also the motor neurons inhibiting the extensor muscles. The lower motor neuron then branches to include several hundreds of muscle fibers, which altogether is called a motor unit (MU). An entire skeletal muscle is composed of many MUs. [Martini, 2006; Silbernagl and Despopoulos, 2009; Merletti and Parker, 2004]

3.2 Voluntary contraction of a skeletal muscle

The muscle fibers of a MU are controlled by the lower motor neuron through a neuromuscular junction located midway along the length of the fiber. When a stimulus arrives at the motor end plate, the permeability of the sarcolemma changes creating an electrical impulse, which quickly spreads across the entire sarcolemma activating all myofibrils in the muscle cell almost instantaneously. This process initiates the contraction cycle, which produces tension through the pivoting of myosin heads, known as the sliding filament theory. However, a single stimulus only produces activation of the MU for a very short duration of time producing only a short muscle twitch. Thus, to produce a movement, several stimuli are required. If the muscle fibers are stimulated immediately after the entire relaxation period has ended, the following twitch will be slightly stronger than the previous. This is known as the treppe phenomenon. However, this approach can only be used to produce approximately a fourth of the maximum muscle tension. Thus, to produce maximum tension, the second stimulation must arrive before the muscle fibers are relaxed, which is the approach normally used by the CNS during normal contraction. This is known as tetanus stimulation. [Martini, 2006]

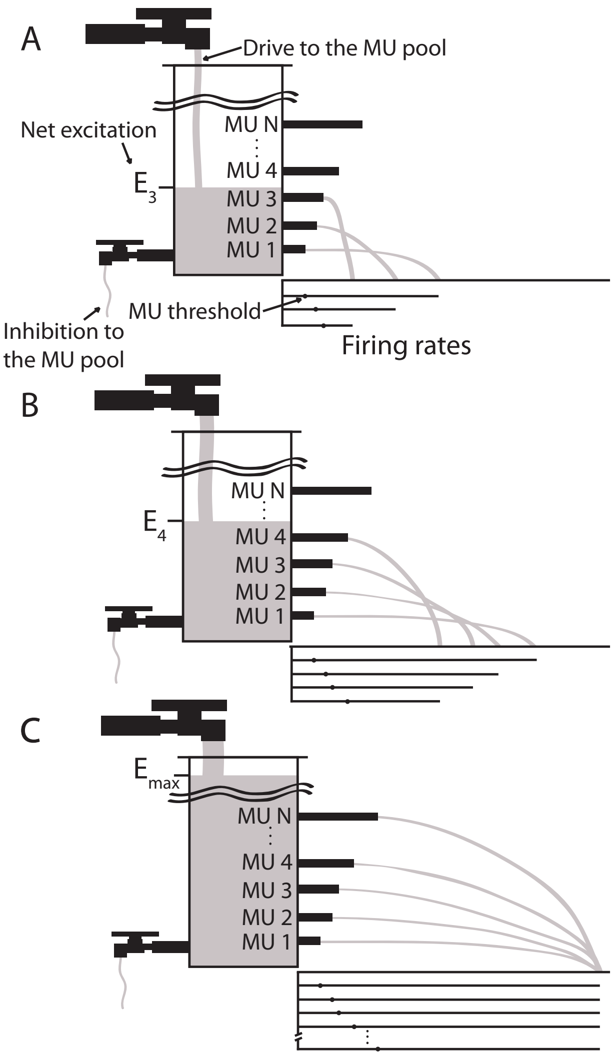

Figure 3.1

A hydraulic model representing the regulation of MUs by the CNS. The common drive is given by the drive into the MU pool subtracted the inhibition. A) shows a common drive just strong enough for activation of three MUs, B) indicates a slightly stronger common drive recruiting an additional MU as well as increasing the firing rate of the already recruited MUs, and C) convergence towards the maximal firing rate of all MUs during maximal common drive (tetanus stimulation). Adapted for own use from Luca and Erim [1994]

Activation of the MUs in a skeletal muscle follows Henneman's size principle, which states that MUs are generally recruited in order of fewest fibers to most fibers during an increase in the strength of the contraction. Through complete tetanus stimulation of all MUs, the peak tension can be reached although only for a brief period. Thus, MUs are activated on a rotating basis, as MUs quickly use their energy reserves, depending on the type of muscle-fibers constituting the MU. This produces an asynchronous activation maintaining a level less than maximum tension. [Merletti and Parker, 2004; Martini, 2006]

In the work by Luca and Erim, a general model for activation of MUs in relation to isometrically produced force was proposed. The model suggests that the activation of MUs is controlled by a common drive (i.e., common stimulation) from the CNS to the muscle rather than an individual control of each single MU, see figure 3.1. The size principle stated by Henneman is explained by different recruitment thresholds of MUs. Thus, for an increasing firing rate from the CNS, increasingly more MUs are activated. This also suggests, that the firing rate of earlier recruited MUs will at any time be larger than later recruited MUs. However, factors such as availability of oxygen and nutrients has also been shown to have an effect causing some MUs to be in a complete relaxation-state, i.e., non-recruitable. [Luca and Erim, 1994; Merletti and Parker, 2004]

3.3 Measurement of myoelectric signals

The electrical impulses conveyed across the sarcolemma of all MUs give rise to myoelectric signals, which can be measured as the EMG. The EMG can fundamentally be measured either non-invasively or invasively. Non-invasively, EMG is measured from the skin using surface electrodes (sEMG) and invasively, EMG is commonly measured using intramuscular wire or needle electrodes (iEMG). An obvious disadvantage of the intramuscular electrodes is the need to be inserted into the muscle, which can cause discomfort and risk of infection. Even though surface electrodes are non-invasive they can cause skin irritation. Furthermore, sEMG may change over time due to change in e.g. skin impedance or electrode lift-off. [Merletti and Parker, 2004]

Albeit both techniques measure myoelectric signals, the pattern of even the same MUs will appear very different. The iEMG signals provides a more detailed local response at the MU level, whereas sEMG collects the global information from several MUs often from several muscles. This is because the action potentials from different MUs pass through the tissue, which act as a low-pass filter. Thus, the pattern measured with sEMG will be broader and with lower amplitude than with iEMG. Moreover, sEMG will contain a summation of several MUs, whereas MUs in iEMG often can be distinguished even at a relatively high contraction level. Consequently, the use of sEMG and iEMG as information sources for myoelectric prosthesis may complement each other rather than being alternatives. [Merletti and Parker, 2004]

Figure 3.2 depicts both the sEMG and the iEMG, top left and right respectively. It can be seen that the iEMG is very localized in time with an amplitude of approximately 2.5 μV, whereas the sEMG is smoothed out by the low-pass filtering characteristics of the skin, and thus has a lower amplitude of 0.5 μV. Furthermore, the iEMG contains high frequency components in the range of 100 to 2500 Hz whereas the sEMG ranges from 20 to 400 Hz, see figure 3.2 bottom. [Komi and Tesch, 1979; Merletti and Parker, 2004]
Typically, only sEMG is considered for control of myoelectric prosthesis. However, for the reasons mentioned above, the use of intramuscular signals has also been suggested by Scheme and Englehart to be useful for control of myoelectric prosthesis; in particular for multiple DoFs and simultaneous movements. Moreover, iEMG sensors can possibly be chronically implanted allowing robust measurements during the day even after doffing and donning of the prosthesis [Scheme and Englehart, 2011].

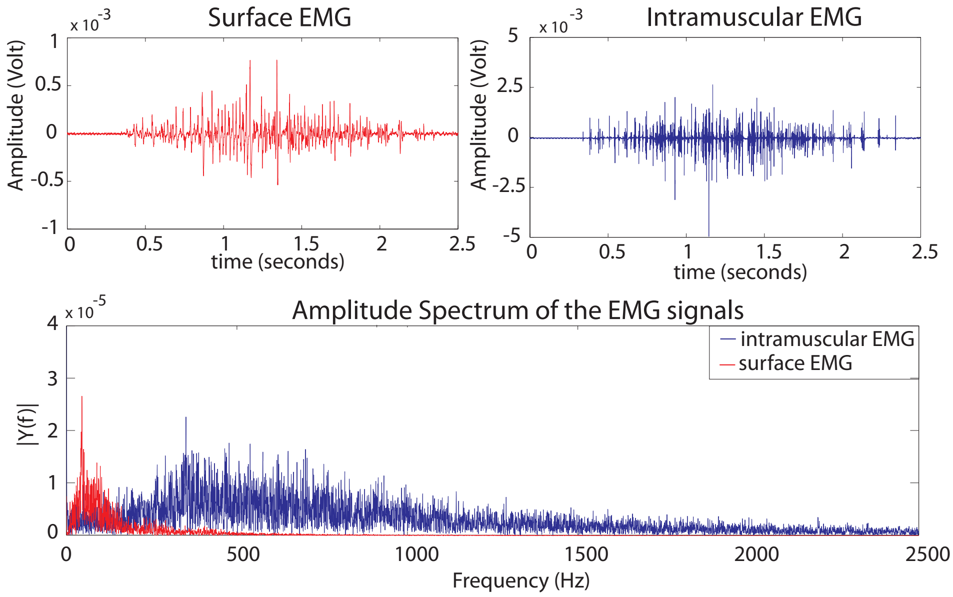

Figure 3.2: Representation of sEMG and iEMG signal and their corresponding frequency content.

Myoelectric control schemes 4

This chapter describes the methods to develop a control scheme. A control scheme is the strategy for converting the EMG into a control signal, which enables the prosthesis to perform intended movements and/or a given force.

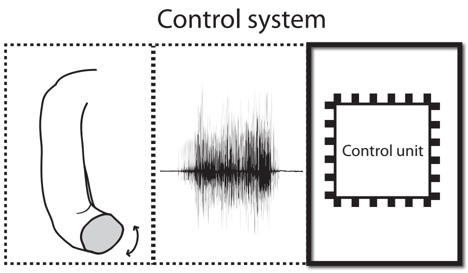

Generally three types of control schemes for prosthetic myoelectric control have been reported in the literature. These are state control, proportional control and pattern recognition [Oskoei and Hu, 2007]. Common for all three control schemes is a preprocessing step. The stages required in the different control schemes can be seen in figure 4.1. Each stage contains different parameters that can be adjusted, which will be described throughout this chapter.

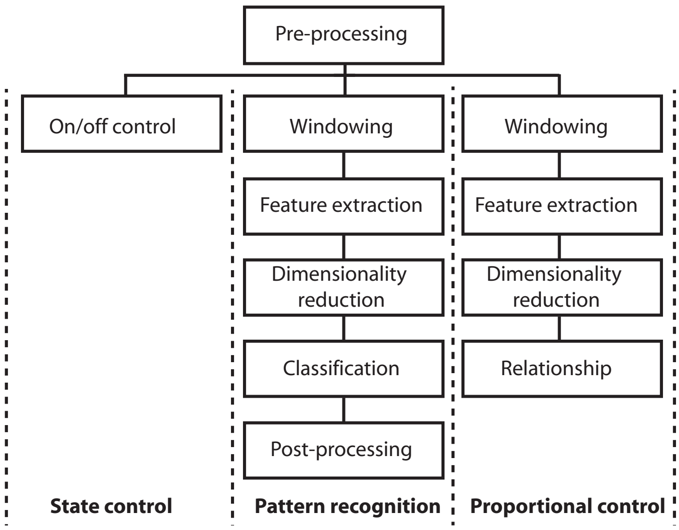

Figure 4.1: The different stages in the control schemes.

Preprocessing

The EMG signal is usually contaminated with unwanted components, e.g., motion artifacts and power line noise, which can be attenuated using a filter. Usually a bandpass filter is used, preserving the EMG signal but removing noise components. [Zecca et al., 2002; Hargrove et al., 2009, 2010; Scheme and Englehart, 2011]

4.1 State control

One of the first myoelectric control schemes to be implemented used the on/off strategy. When the EMG exceeds a specified threshold the prosthetic device turns on a defined function, for example, closing the hand, see figure 4.2. This strategy can be used to control a number of states or functionalities by defining different thresholds corresponding to different functions, or alternatively by having independent sources for different functions. [Battye et al., 1955; Bottomley, 1965; Scott, 1967; Parker et al., 2006; Merletti and Parker, 2004]

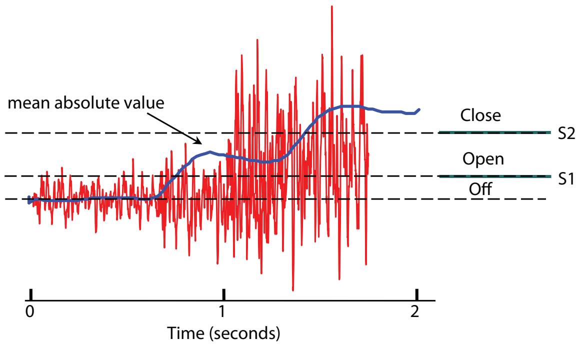

Figure 4.2: State control of a prosthetic hand. When the value of the EMG signal increases above predefined thresholds different functions of the hand are turned on - in this case open and close. [Parker et al., 2006]

A three state control scheme was developed by Dorcas and Scott using one EMG channel from the biceps brachii. One contraction level corresponded to activation of function one and a higher contraction level to function two. In clinical evaluation only a short training period was sufficient to achieve reliable control using this particular approach [Dorcas and Scott, 1966].
The on/off strategy has been expanded for control of up to five states by Paciga et al. obtaining error rates as low as 1.1 % when switching between states. However, users were provided with visual feedback on contraction level, which is not feasible in practice [Paciga et al., 1980].

4.2 Pattern recognition

Pattern recognition is a control scheme where observations from input signals are assigned to a class in a predefined set of classes. An observation typically consists of multiple features, which represent characteristics of the signal. To map observations to classes, a learning procedure that trains the classifier in separating observations is used, see figure 4.3 [Duda et al., 2000]. In myoelectric control, the observations are extracted from the EMG signal and the classes are represented by the movements. To allow discrimination of the intended movements, a number of processing stages must be completed. These are windowing, feature extraction, and classification. The different steps all impact how well the control scheme assigns observations from the EMG signal to intended movements, which is quantified as a classification accuracy. These are thus important to consider in a pattern recognition based control scheme. Furthermore, two optional steps can be taken to improve classification accuracy, which are dimensionality reduction and post-processing. [Oskoei and Hu, 2007; Hargrove et al., 2009, 2010; Zecca et al., 2002]

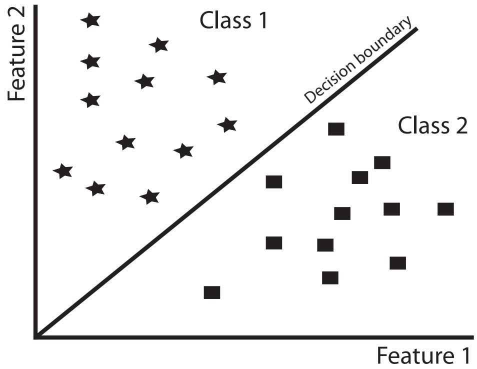

Figure 4.3: Basic concept of pattern recognition, were observations are assigned to class 1 or class 2 based on the decision boundary.

4.2.1 Windowing

Before extraction of features, a segment of the EMG signal has to be selected since the instantaneous EMG value is not appropriate for classification. The segment is selected by multiplying a window with a certain length (usually 50-400 ms) to the EMG signal. The length of the window determines the stability of the features, where a long window will produce more stable features improving classification accuracy. However, applying a longer window will also create a longer delay of the system, which has to be considered for prosthetic use. Additionally, windows can be specified to overlap in order to create a denser stream of classifications, where the size of overlap is limited by the processing speed of the system. [Hargrove et al., 2010; Scheme and Englehart, 2011; Englehart and Hudgins, 2003; Oskoei and Hu, 2008]
It has been shown by Englehart et al., that the state of the EMG signal compared to window length and classification accuracy is of importance. If the transient state (onset of contraction or rapid changes in contraction level) of the EMG signal is used, the impact of the window length on classification accuracy is larger as compared to the steady state of the EMG signal - especially for short window lengths. [Englehart et al., 2001]

4.2.2 Feature extraction

A segment of the EMG signal determined by the window is used to extract a number of different features. A large number of features have been used, which can roughly be divided into three domains: time domain (TD), frequency domain (FD) and time-frequency domain (TFD). [Oskoei and Hu, 2007; Zecca et al., 2002]

Time domain features
TD features are based on EMG amplitudes, which makes them computationally inexpensive. This property is preferable in myoelectric control, where processing time and power consumption is important. TD features that have been used extensively throughout the literature especially for sEMG, although also for iEMG, are: Variance (VAR), mean absolute value (MAV), mean absolute value slope (MAVSLP), root mean square (RMS), Willison amplitude (WAMP), zero crossing (ZC), slope sign changes (SSC) and waveform length (WL). [Oskoei and Hu, 2007; Zecca et al., 2002; Oskoei and Hu, 2006; Kamavuako et al., 2012]

Frequency domain features
FD features are based on the power spectrum density (PSD) and not the amplitude of the EMG signal, which makes them computationally more expensive. However, using FD features in a control scheme provides different information from the EMG signal. The frequency features that have been used are mean frequency (MNF), median frequency (MDF), frequency ratio (FR) and auto regressive (AR) coefficients, where especially AR coefficients have been commonly used in the literature [Oskoei and Hu, 2006; Hargrove et al., 2007].

Time-frequency domain features
Normally when applying FD features, the EMG signal is assumed stationary within each window. However, especially during the transient states of the EMG, this assumption might not be valid. Therefore, TFD features have also been investigated, although only for sEMG. [Oskoei and Hu, 2007; Zecca et al., 2002]
Features of the TFD that have been used are: Short time Fourier transform (STFT), wavelet transform (WT) and wavelet packet transform (WPT). The STFT has a uniform resolution in both time and frequency, whereas the wavelet based features does not impose uniform resolution in time and frequency. [Oskoei and Hu, 2007; Zecca et al., 2002]

Impact of features on classification accuracy
Oskoei and Hu compared all the mentioned TD features to the FD features MNF, MDF and FR and found that single TD features outperformed single FD features. Albeit, this same pattern was found by Phinyomark et al., it was shown that the FD features MNF, MDF and FR was outperformed by the FD feature mean power (MP). [Oskoei and Hu, 2006; Phinyomark et al., 2012]

In a study by Englehart et al. TFD features (STFT, WT and WPT) were compared to TD features for transient sEMG signal. Here, it was shown that the TFD features resulted in increased classification accuracy compared to TD features after dimensionality reduction (explained in the next section) of the feature space. These results were later confirmed by the same author for both transient and steady-state EMG signal [Englehart et al., 1999, 2001].
Khezri and Jahed investigated the influence of wavelet parameters on sEMG signals

and found that using the biorthogonal 3.5 wavelet with 9 levels of decomposition provided the best performance. However, the daubechies 2 and symlet 2 and 9 showed almost as good performance. Additionally, Englehart et al. used both the coiflet 4 and the symlet 5 mother wavelet obtaining high classification accuracies. [Khezri and Jahed, 2007; Englehart et al., 1999]

Oskoei and Hu evaluated classification accuracy in relation to feature selection and segment length on sEMG signal. It was found that single TD features were less affected by segment length and showed better general performance compared to single AR features of the FD. [Oskoei and Hu, 2008]
Combined features (combined TD features compared to combined TD+AR features) were also investigated and showed to have higher performance than single features for short segment lengths. [Oskoei and Hu, 2008]
Another study by Huang et al. showed that combining AR features with TD features resulted in a higher classification accuracy than TD features alone. Hargrove et al. assessed sEMG versus iEMG using combined TD and AR features and found comparable classification accuracy for the two signals using these features. [Huang et al., 2005; Hargrove et al., 2007]

Many different feature combinations have been used in the literature, but there is no obvious tendencies of which features perform best in general. However, using a combination of features from different domains seems to provide the most generic results.

4.2.3 Dimensionality reduction

As can be seen from the above section, many different features can be chosen and combined. However, a very large number of features (each providing a dimension in the feature space) can lead to a problem referred to as "the curse of dimensionality", which states that a large feature space requires more training data. A way to reduce the dimensionality is through principal component analysis (PCA). This technique maps the feature space to a lower dimension, while keeping as much variance as possible [Oskoei and Hu, 2007]. PCA has been used extensively in the literature and has been shown to increase classification accuracy. [Englehart et al., 1999, 2001; Hargrove et al., 2007, 2009; Khezri and Jahed, 2007]
However, albeit not used extensively in literature, other methods such as separability and correlation (SEPCOR), where separability is preferred above variance, do exist. [Ege et al., 2000]

4.2.4 Classification

To classify different movements for myoelectric control, different classifiers with different properties have been proposed. Among the different classifiers can be mentioned linear discriminant analysis (LDA) and the more complex multilayer percep-

tion artificial neural network (ANN). [Englehart et al., 1999, 2001; Englehart and Hudgins, 2003; Hargrove et al., 2010]
Interestingly, in a study by Englehart et al. LDA was shown to outperform the more complex ANN, which may be due to the to the linearizing effect of the PCA. [Englehart et al., 1999]

Another type of classifiers are based on fuzzy logic, where expert knowledge can be incorporated in an if-else classification structure, which is advantageous if a rule base can be created [Ajiboye and Weir, 2005; Oskoei and Hu, 2007]. An extension of the fuzzy logic approach is the neuro-fuzzy classifiers that combine knowledge about the system from the fuzzy approach with the ability to train the classifier using the neural networks [Khezri and Jahed, 2007; Zecca et al., 2002].

Yet another classifier is the support vector machine (SVM). This classifier is originally intended for binary problems but has been adapted to differentiate between multiple classes. The approach is to train one classifier for every combination of two classes and use a one against one principle. Alternatively, each binary classifier is trained on one class versus the remaining classes in a one against all approach. [Oskoei and Hu, 2008]

Hidden Markov Models (HMM) and Gaussian Mixture Models (GMM) have also been used for classification purposes but were shown to have the same classification accuracy as ANN and LDA for a sixth order AR feature set by Hargrove et al.. [Hargrove et al., 2007]

It has been shown that choosing the proper features and performing PCA makes the classification task minimally dependent on the choice of classifier. [Scheme and Englehart, 2011; Scheme et al., 2011]

Reference	Class	Channels	Classifier	Features
Englehart et al. [1999]	4	2 sEMG	LDA, ANN	MAV, MAVSLP, ZC, SSC, WL, STFT, WT, WPT
Englehart et al. [2001]	6	4 sEMG	LDA, ANN	MAV, MAVSLP, ZC, SSC, WL, STFT, WT, WPT
Englehart and Hudgins [2003]	4	4 sEMG	LDA	MAV, MAVSLP, ZC, SSC, WL
Ajiboye and Weir [2005]	4-5	3-4 sEMG	Fuzzy logic	-
Huang et al. [2005]	6	4 sEMG	LDA, ANN, GMM	MAV, RMS, ZC, SSC, WL, AR
Hargrove et al. [2007]	10	16 sEMG, 6 iEMG	LDA, ANN	MAV, RMS, MAVSLP, ZC, SSC, WL, AR
Khezri and Jahed [2007]	6	4 sEMG	Neuro-fuzzy	MAV, SSC, AR, WT
Oskoei and Hu [2008]	6	4 sEMG	LDA, ANN, SVM	MAV, RMS, WL, VAR, ZC, SSC, WAMP, AR, MNF, MDF
Hargrove et al. [2009]	11	10 sEMG	LDA	AR
Scheme et al. [2011]	6-11	10 sEMG	kNN, SVM, ANN, GMM, LDA	MAV, MAVSLP, ZC, SSC, WL

Table 4.1: Chronological overview of the references used for pattern recognition including methodological aspects of the experimental designs. All studies achieved high accuracies (above 90 %) with at least one of their approaches.

4.2.5 Post-processing

After classification, a post-processing step can be utilized on the classification stream. One way is by performing a majority vote (MV), which takes a number of results from the classifier and classifies the movement as the class with most occurrences. This can improve classification accuracy but at the cost of response time. If overlapped windows are used and the step is chosen to equal the processing delay of the system the densest stream of classifications is produced. Consequently, more results are available for the majority vote. [Englehart and Hudgins, 2003; Chan and Englehart, 2005]

A short overview of the references used in the description of the stages of pattern recognition control scheme can be seen in table 4.1. The table describes the number of information sources (EMG channels), the complexity of the control scheme (classes), the classification approach and the utilized features.

4.3 Proportional control

To enable determination of not only the intended movement but also the force of the movement, another control scheme called proportional control has been utilized. In the proportional control scheme, a relationship between the activity of the EMG signal and force is determined, see figure 4.4. This allows prosthetic devices to be controlled not only for different DoFs, but also to determine the intended force that the prosthetic hand should perform. [Dorcas and Scott, 1966; Englehart et al., 2001; Cotton et al., 2007]
As with pattern recognition, for proportional control the data must be windowed and representative features extracted before a relationship between the features and force can be determined.

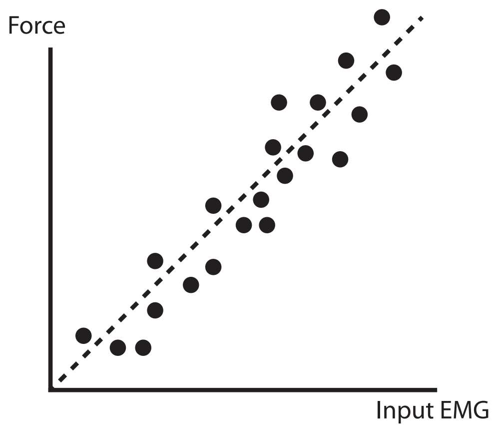

Figure 4.4: Proportional control of prosthesis. Force is dependent on EMG variables. In this case force increase linearly with increasing EMG value.

4.3.1 Windowing

Kamavuako et al. investigated the relationship between grasping force and single channel sEMG and iEMG. It was found that the significantly highest correlation between force and sEMG could be obtained using a 200 ms window and a 300 ms window for iEMG [Kamavuako et al., 2009]. Another study by Nielsen et al. used seven sEMG channels to estimate force for simultaneous movements of two wrist DoFs. The window length that resulted in the highest correlation between sEMG and force in this case was found to be 100 ms. [Nielsen et al., 2011]

4.3.2 Feature extraction

In the literature many authors use the amplitude of the EMG signal to estimate the force produced. Basic 5 Hz low pass filtering of the rectified EMG signal, integration of the rectified signal, moving average (MA), moving average root mean square (MARMS) and mean square value (MSV) have been used. [Hoozemans and van Dieën, 2005; Onishi et al., 2000; Jiang, 2009; Kamavuako et al., 2009]
A multi-dimensional feature space has also been investigated in the study by Nielsen et al. resembling that of pattern recognition based movement classification. The feature used by Nielsen et al. were a combination of the TD features MAV, ZC, SSC and WL, which were also combined with AR or WT features. Here, the combined TD features outperformed the MSV single feature. However, combining TD and AR or WT did not improve performance any further. [Nielsen et al., 2011]
In a study by Kamavuako et al. nine TD features were investigated in all possible combinations. The best performance could be obtained combining the WL, SSC, WAMP, modified-MAV, and constraint sample entropy (CSE) features [Kamavuako et al., 2012].

4.3.3 Relationship

Both linear and nonlinear relationships has been proposed in the literature [Kamavuako et al., 2009; Nielsen et al., 2011]. Even though the ANN should fit the data in the best possible way theoretically, a linear model (LM) has shown to produce similar results for one-channel sEMG and iEMG and grasping force [Rosenvang et al., 2010b].

4.4 Pros and cons of myoelectric control schemes

To distinguish between multiple movements, especially a pattern recognition control scheme has been used in the literature, whereas proportional control has proven effective for force estimation. Common is that the choice of parameters, e.g. features, have varied between different control schemes proposed by different authors and, consequently, it is not clear which parameters provides the best results in general [Farrell and Weir, 2008a].

The three control schemes: state control, pattern recognition and proportional control have been reviewed. Each of the control schemes has some advantages and disadvantages, which have been explained in this chapter and are summarized in table 4.2.

Control scheme	**Prospects**	**Consequences**
State control	Simple Fast Clinically available	Allows few DoFs Limited by predefined thresholds Must have independent control sites
Pattern recognition	Allows many DoFs Can be fast Allows intuitive control Can use untargeted electrode sites	Must be trained Advanced schemes are slow Limited by predefined classes
Proportional control	Continuous force estimation Simple Allows intuitive control	Allows few DoFs Predefined input-output relationship

Table 4.2: Prospects and consequences of each of the three control schemes: state control, pattern recognition and proportional control.

5 Aim

Throughout the problem analysis, several important factors for control of myoelectric prosthesis have been investigated. The initial problem statement concerned improvement of the control, and many factors have been disclosed throughout the analysis. The control system for a prosthesis consists of the following steps:

- Locating a source of myoelectric signals
- Identifying the information available in the signal
- Extracting and applying information from the signal for control

According to the initial problem statement, the goal was to improve the control system to allow simultaneous control of multiple DoFs with corresponding force estimation. In order to do so, a number of choices was made with basis in the knowledge established in the problem analysis.

Locating a source of myoelectric signals

In chapter 2 it was found that different muscles map different movements of the hand. However, amputation affects this relationship, since some muscles are completely lost, and the anatomy of the remaining muscles change due to the amputation. Thus, for amputees no unique mapping can be made between muscles and movements. However, untargeted techniques have shown comparable results to targeted techniques for control of single movements, which potentially eliminates the need to use a specific mapping between muscles and movements. The use of a untargeted technique has not been investigated for control of simultaneous DoFs or estimation of force. Thus, it was chosen to use an untargeted technique to investigate its potential use for simultaneous movements and force estimation. Moreover, the use of untargeted measurement sites would also ease the possible future design of a prosthesis.

Three movements of the hand and wrist were identified to be the most important to regain for an amputee: 1) flexion/extension of the fingers, 2) pronation/supination of the wrist, and 3) flexion/extension of the wrist. Thus, it was chosen to support these movements in the control system.

Identifying the information available in the signal

In chapter 3 the content of the EMG was investigated, where a relation between the size of the common drive activating MUs and the produced force was found. To measure the activity of the MUs, two recording techniques were identified, namely sEMG and iEMG. sEMG provides a more global representation of the muscle activation, whereas iEMG provides a more localized representation. Therefore, it was chosen to use both sEMG and iEMG, which can provide information on muscle activation together with the force produced by the muscles.

Because of the different characteristics of sEMG and iEMG, it was chosen to compare these when developing the control system for simultaneous DoFs. Furthermore, in chapter 3 it was argued that the two information sources should not necessarily be compared but also combined, as they may complement each other rather than being alternatives. Thus, it was also chosen to combine sEMG and iEMG to assess whether this could provide better results.

Extracting and applying information from the signal for control
Chapter 4 found that a myoelectric control scheme is necessary to convert the information in the EMG to the control signal for the prosthetic device.
For classification of movements, especially pattern recognition based control schemes were found to be useful whereas proportional control schemes have shown to be good for estimation of force.
To our best knowledge, no work has been published using a hybrid between proportional control for force estimation and pattern recognition for movement classification (for both single and simultaneous DoFs). As the current project aims at investigating both simultaneous movements along with force estimation, a hybrid control scheme was chosen.
The hybrid control scheme has a number of stages, each containing different parameters that can be adjusted, see figure 5.1. A special property of the hybrid control scheme is, that there can be an interaction between the force estimation and the movement classification, i.e. the result from the classifier may be used in the force estimation and vice versa.

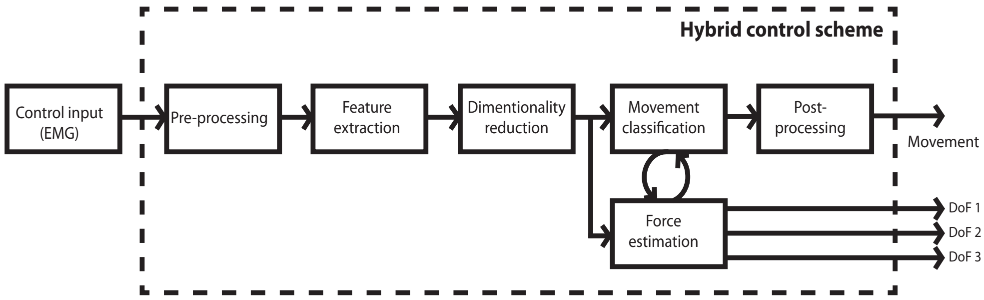

Figure 5.1: Stages of the proposed hybrid control scheme.

The choice of parameters, e.g. features, used in the different control schemes has varied between authors, and consequently no apparent choice regarding these could be made. Therefore, it was chosen to investigate which parameters provided the optimal results for the proposed hybrid control scheme.

It was chosen to investigate the effect of different window sizes, different TD, FD, TFD features and a combination of feature domains. Moreover, both PCA and SEPCOR algorithms were investigated as dimensionality reduction techniques to identify

the optimal method.
It has been shown that the choice of classifier has a minimal effect on the performance of a control scheme, if appropriate features are selected. However, it was chosen to investigate which of the following four common classifiers (LDA, kNN, SVM and ANN) was the most suited for the particular control scheme. Moreover, the effect of adding post-processing to the outcome from the classifier was investigated.
The relation between both sEMG and iEMG, and force was found to be well-described using a proportional control scheme based on an ANN. However, a LM approach has also shown to perform equally well for a more simple case and thus it was chosen to investigate which of these methods could provide the best results.

5.0.1 Choices summarized

The choices made for the control system based on the problem analysis can be seen in figure 5.2.

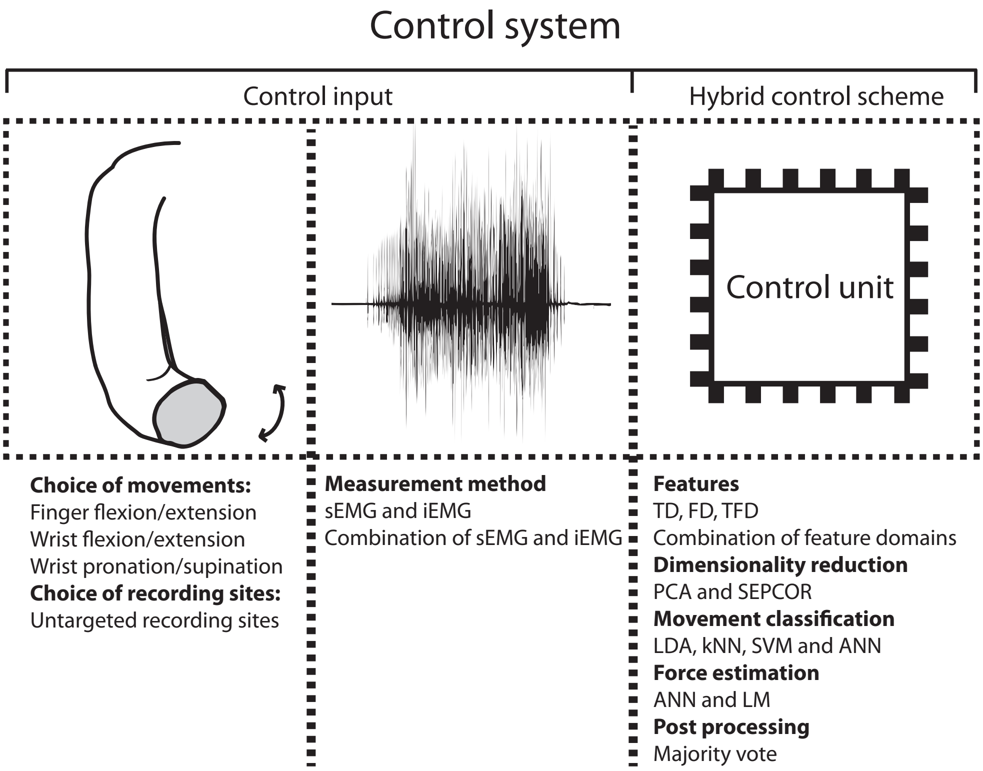

Figure 5.2: Choices made on basis of the problem analysis according to the steps in designing the control system.

Hypothesis

A novel hybrid control scheme based on untargeted EMG signals (iEMG and sEMG) will allow precise, simultaneous control of finger flexion/extension, wrist flexion/extension and wrist pronation/supination movements along with corresponding force.

Experiment

II

6 Experimental design

Based on the analysis, a number of choices were made resulting in the proposed hypothesis. In order to test this hypothesis, an experiment was conducted. To do so, a number of additional choices relating to the execution of the experiment were made. This chapter describes these choices with corresponding arguments and the used protocol.

6.1 Subjects

The study included 10 healthy subjects (6 men / 4 women, mean age: 24.4 [range: 23-26]) with no limb deficiencies or neurological disorders. The protocol was approved by the Danish local ethical committee (approval no.: N-20080045). Prior to the experiment, subjects were given both oral and written information about the experiment as well as signing a written consent. All subjects were made aware that participating was voluntary and that they could resign at any point during the experiment.

6.2 Degrees of Freedom

In the analysis, it was chosen to investigate the three DoFs: finger flexion/extension, wrist flexion/extension and wrist pronation/supination. However, no available devices for measuring force (dynamometers) for all three DoFs existed. An attempt to design a dynamometer allowing both finger flexion/extension and wrist pronation/supination has been made by Rosenvang et al. using multiple transducers. However, the results showed inconsistent output from the transducers. Thus, in this study it was chosen to develop a dynamometer based on a single, precise, multiaxial transducer (Gamma FT-130-10, ATI Industries), and, consequently, it was only possible to measure wrist DoFs. Therefore, finger flexion/extension was excluded leaving the two wrist DoFs flexion/extension and pronation/supination. To allow simultaneous control of the two wrist DoFs, they were combined, resulting in four the movements: simultaneous flexion and supination (flexion+supination), simultaneous extension and pronation (extension+pronation), simultaneous flexion and pronation (flexion+pronation), and simultaneous extension and supination (extension+supination). Thus, in total 8 different movements were included:

- Flexion
- Extension

- Pronation
- Supination
- Flexion+supination
- Extension+pronation
- Flexion+pronation
- Extension+supination

An additional consequence of the design of the dynamometer was, that the performed movements produced a torque in the transducer and thus forces were represented by moments of force.

6.3 EMG acquisition

In a study by Hargrove et al. applying a total of 16 sEMG channels, classification accuracy was compared to the number of EMG channels. It was shown that only three channels were needed to obtain the maximal classification accuracy, if the three optimal channels were selected. A symmetrical channel selection was also performed using equally spaced channels around the forearm, where four channels resulted in maximal classification accuracy. While classification accuracy did not improve by raising the number of channels for sEMG above four, similar performance was observed as a result of utilizing six iEMG channels. Since no studies have utilized untargeted techniques for force estimation, it was decided to use six iEMG channels and six sEMG channels based on the studies for movement classification. [Hargrove et al., 2007; Farrell and Weir, 2008a]

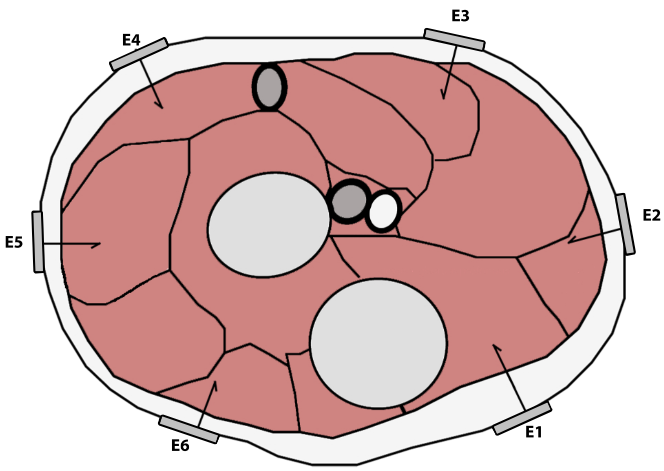

Figure 6.1: Example of sEMG and iEMG placement at equally spaced distances around the forearm starting just lateral of the ulnar exposure. iEMG was inserted at a 45° angle oriented in the proximal direction, such that sEMG electrodes were placed approximately above the tip of the iEMG electrodes. Electrode position in relation to muscle anatomy as shown on the figure was not necessarily the same for all subjects due to the untargeted electrode placement technique.

The EMG electrodes were placed according to the protocol used by Farrell and Weir in a circle around the forearm at approximately 1/3 distal of the elbow joint [Farrell and Weir, 2008a].
The sEMG electrodes (Ambu Neuroline 720) were placed equidistantly, starting just lateral of the ulnar exposure.
For iEMG (custom-made by use of hypodermic needles, 25G from B. Braun, and Teflon coated wires from AM-Systems), an insertion angle of 45° was chosen with the orientation of the needle parallel to the arm and in the proximal direction. An approximate insertion depth was chosen as the circumference of the arm divided by 16 [Farrell and Weir, 2008a]. Prior to insertion of the needle, the area was sterilized with alcohol to minimize the risk of infection. iEMG electrodes were placed immediately distal to each sEMG electrode. Electrode placement was verified based on the presence of EMG signal during contraction of all forearm muscles during various movements.

6.4 Force profiles for execution of movements

The experiment was composed of three trials in total. The purpose of the first two trials was to collect data while performing all movements similarly, while the third trial consisted of a less ideal execution of the movements. In order to create a consistent, uniform execution of the different movements throughout the experiment, it was chosen to use a standardized force profile for each movement. The movements were performed isometrically by exerting a force in the direction of each movement, which was measured by the dynamometer. [Kamavuako et al., 2009; Bøg et al., 2011]
To include different force levels, it was chosen to use a dynamic force profile for each movement. To incorporate a more natural use of a prosthesis into the force profile, it was chosen to switch directly from one movement to another [Parker et al., 2006]. This was also done in a study by Nielsen et al., where sinusoidal force profiles were used for control of two single and simultaneous DoFs. Thus, in the present study it was chosen to use sinusoidal profiles, since they incorporate dynamic force levels with shifting movements. The sinusoidal profiles were chosen to oscillate at a frequency of 0.25 Hz as used by Nielsen et al.. This resulted in one force profile for each single DoF:

- Flexion followed by extension, see figure 6.2 a)
- Pronation followed by supination, see figure 6.2 b).

Furthermore, two profiles were made to cover the simultaneous DoFs:

- Flexion+pronation followed by extension+supination, see figure 6.2 c).
- Flexion+supination followed by extension+pronation, see figure 6.2 d).

For the third trial, a force profile was made for each single and simultaneous DoF. However, as this trial should represent a less ideal case, the force profiles were amplitude and frequency modulated (frequency range 0.1-0.5 Hz, amplitude range 0.5-2

Nm). All profiles were set to have a duration of 30 s to avoid muscle fatigue during the task.

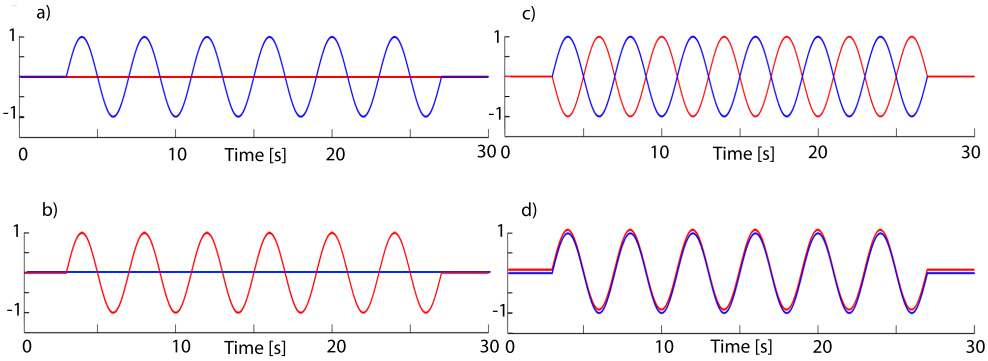

Figure 6.2: The figure depicts the profiles for a) the single DoF flexion and extension, b) the single DoF pronation and supination, c) the simultaneous DoF for flexion+pronation followed by extension+supination, and d) the simultaneous DoF for flexion+supination followed by extension+pronation.

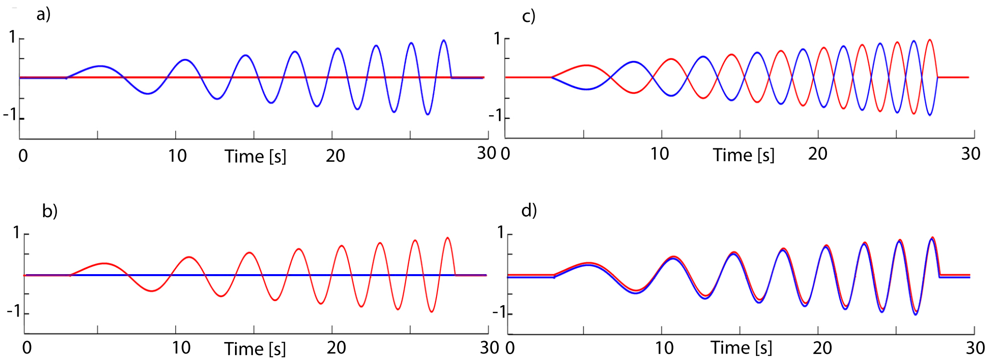

Figure 6.3: The figure depicts the frequency and amplitude modulated profiles (Frequency range: 0.1-0.5 Hz, Amplitude range: 0.5-2 Nm) for a) the single DoF flexion and extension, b) the single DoF pronation and supination, c) the simultaneous DoF for flexion+pronation followed by extension+supination, and d) the simultaneous DoF for flexion+supination followed by extension+pronation.

Since maximum voluntary contraction (MVC) could not be measured due to a limited force range of the used dynamometer, a percentage of each subject's MVC could not be used as the maximum force level. Therefore, a maximum force level was chosen to be 3 Nm or 2 Nm (for male or female, respectively) for flexion and extension and 2 Nm or 1.5 Nm for supination and pronation empirically verified as a comfortable level of contraction at low to medium force. [Nielsen et al., 2011]
During the experiment, subjects were provided with visual feedback of exerted and targeted force. The force channels corresponding to the DoFs flexion/extension and pronation/supination were represented as blue and red, respectively. Throughout the experiment, the force channels were normalized according to their targeted force profiles such that they appeared similar only differentiated by color, see figure 6.2. Empirically, this was shown to reduce the cognitive load of the task.

6.5 Setup

6.5.1 Positioning of the hand

To enhance consistent muscle activity during the different profiles, the hand was secured firmly in the dynamometer. This was ensured by fixating the hand between two plates. The plates were foam coated to minimize discomfort and to adapt the shape of the plate to the hand of each individual, see figure 6.4. The dynamometer was rotated to fit the shape and angles of the arm and hand better. The hand was inserted creating a distance between the center of the transducer and the joint of the wrist of approximately 5 cm. Moreover, the hand was placed in the upper part of the dynamometer with the thumb above the plates. Markers were made on the hand to ensure consistent location of the hand.

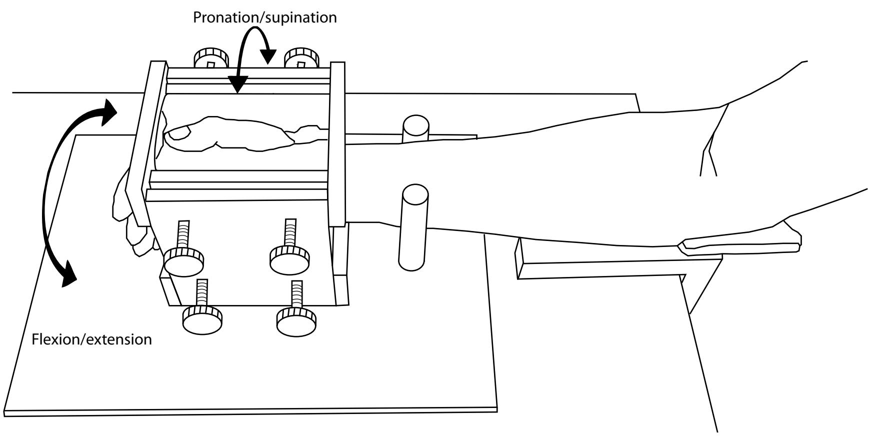

Figure 6.4: Positioning of the subject's arm and hand in the dynamometer as well as directional markers for the used movements.

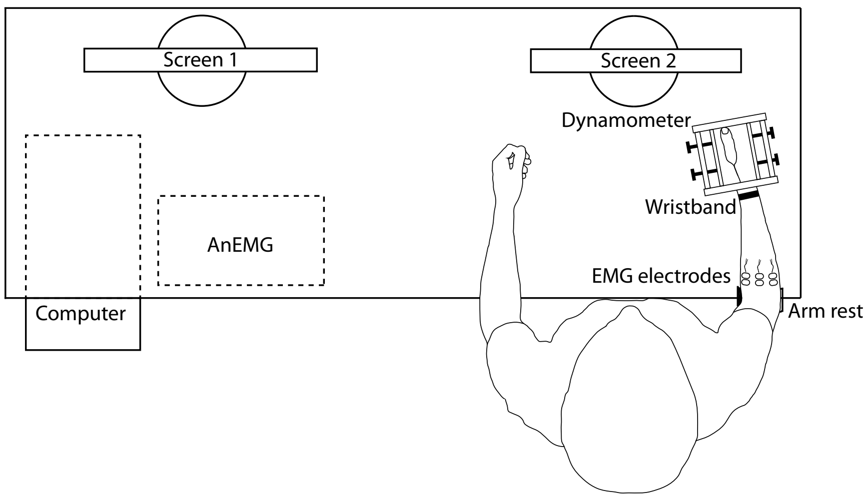

Figure 6.5: Positioning of the subject during the experiment.

6.5.2 Positioning of the subject

The subject was placed on a comfortable chair in an upright position with the elbow fixated in an arm rest, see figure 6.5. The subject faced the screen (screen 2) providing visual feedback for the subject. The experimenter sat next to the subject inspecting all acquired signals on another screen (screen 1) whilst providing guidance for the subject throughout the experiment.

6.5.3 Recording tool

To sample EMG and force data, while providing the subjects with visual feedback of the exerted force in real time, a software tool was developed by the project group. Furthermore, the tool allowed inspection of the EMG signals during execution of the movements. The software tool displayed two windows. Window one, see figure 6.6, enabled the experimenter to control actions (initiating recording, randomizing profiles, saving data etc.) and provided visual real time force feedback for the subject. Window two, see figure 6.7, enabled the experimenter to inspect all 12 EMG channels during profile execution in real time to ensure that all EMG channels were functioning correctly. In order not to confuse the subject, window two was displayed on a separate screen. The software tool also ensured randomization of the order of the profile and a consistent naming of the acquired EMG and force data. All data was sampled at 10 kHz.

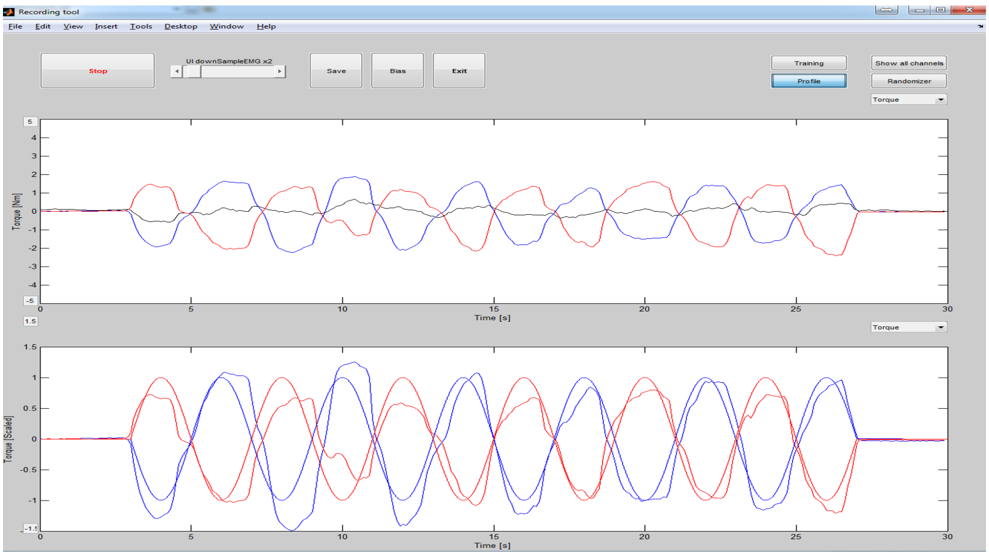

Figure 6.6: A screen-shot of window one in the recording tool, which allow control of multiple functionalities while providing the subject with visual feedback of the exerted force along with the targeted force profile (lower plot).

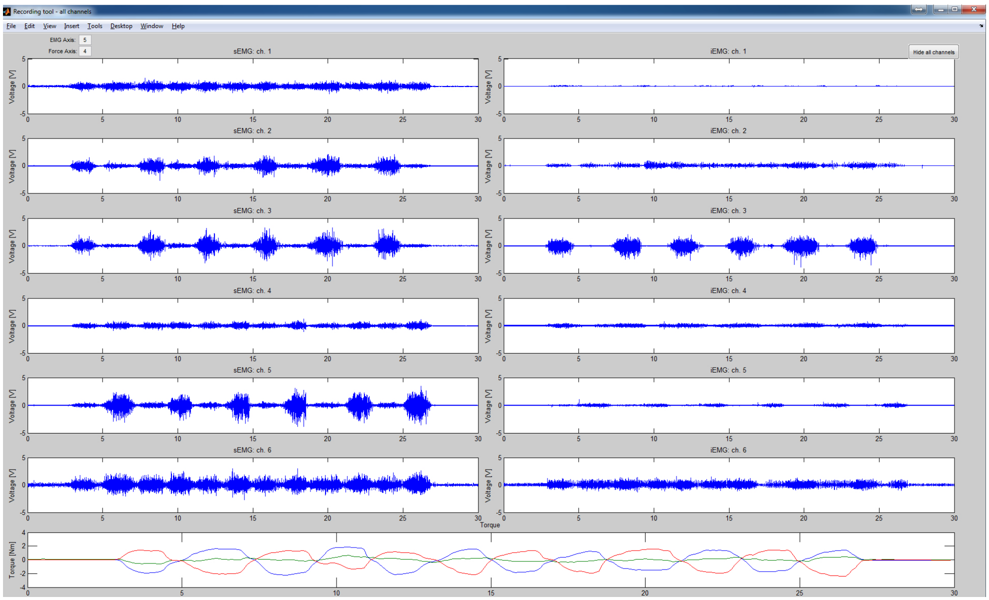

Figure 6.7: A screen-shot of window two in the recording tool, which displays all measured signals for the experimenter in real time (sEMG: left side, iEMG: right side, torque: bottom).

6.6 Procedure

The procedure of the experiment is described below and can be seen in figure 6.8:

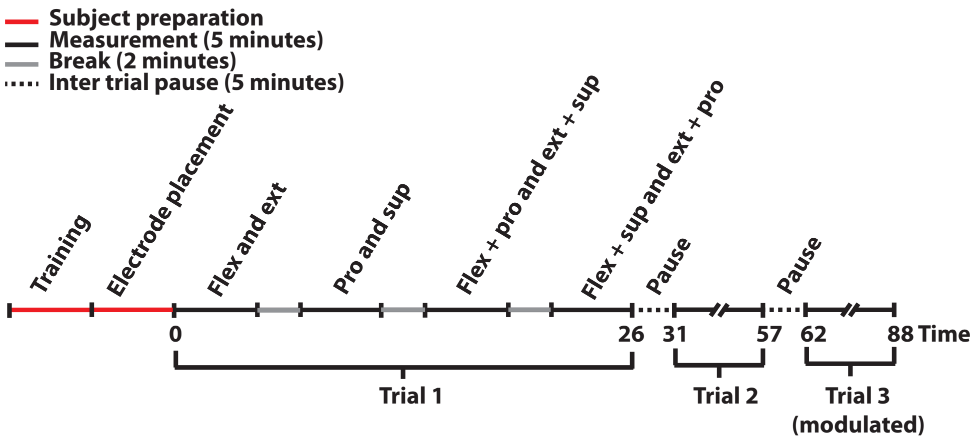

Figure 6.8: Timeline of the experiment. Each measurement was preceded by a break in order to avoid muscle fatigue. Each trial consisted of following the four profiles constituting the eight movements. Each trial was preceded by a 5 minute pause and the two normal trials were completed. Trial three consisted of one repetition of all four profiles as normal trials but with amplitude and frequency modulated profiles.

1. EMG device (AnEMG12) and computer was turned on
2. Recording software was set up
3. Subject was informed about the risks of the experiments and the experiment in general
4. Informed consent was signed
5. Subject's hand was positioned in dynamometer
6. Subject was instructed in performing the movements
   (a) Every profile was trained until a good match between the targeted and the actual force was achieved
7. Subject's hand was removed from the dynamometer
8. Subject's arm was prepared
   (a) Electrode placement was marked
   (b) Electrode area was shaved
9. sEMG electrodes were applied and connected to the AnEMG
10. Correct sEMG electrode placement was verified by presence of sEMG signal during contraction
11. iEMG electrodes were inserted after sterilization of insertion area and connected to the AnEMG
12. Correct iEMG electrode placement was verified by presence of iEMG signal during contraction
13. Subject's hand was positioned in dynamometer
14. Trial 1 was initiated
    (a) Profile order was randomized by the recording software
    (b) Subject performed the current profile and the best match was selected within an approximate 5 minutes time frame including breaks
    (c) Subject was given 2 minutes break
    (d) Step (a) to (c) was repeated for all profiles
    (e) Trial 1 ended and subject was given a pause of 5 minutes
15. Trial 2 was completed as trial 1
16. Trial 3 was completed as trial 1 and 2 with modulated profiles
17. Subject's hand was removed from dynamometer
18. EMG electrodes were removed

Data Processing 7

In order to develop the control scheme proposed in the hypothesis, several processing techniques were implemented for the data acquired in the experiment. These are described in the following.

7.1 Filters

To minimize the effect of noise outside the frequency bands for sEMG and iEMG, a Butterworth band-pass filter was implemented. This infinite impulse response filter was chosen as it has a flat frequency response within the passband and thus has a minimal effect on the EMG signal. The order of the filter was 4 and thus the gain was -24 dB/octave. To avoid removing any frequency components of the signals cut-off frequencies of 20-500 Hz and 100-3000 Hz for sEMG and iEMG were used, respectively.
Moreover, a low-pass Butterworth filter of order 4 was added to the torque signals with a cutoff frequency of 3 Hz, which is well above the maximum frequency of the performed sinusoidal profiles (0.5 Hz).

7.2 Features

To represent the EMG signal, several features were chosen. Each feature was calculated for each channel within a certain window (usually with a length between 50-400 ms.) with some overlap between windows to create a denser stream of outputs.
For the torque channels, the mean torque was calculated for each channel as a feature for each window representing the real performed torque.

7.2.1 Time-domain features (TD)

All the TD features were calculated directly from the EMG signal according to the formulas given below.

Mean Absolute Value (MAV)

MAV is commonly used to detect onset of EMG signal and represents the amplitude of the signal. It is defined as: [Phinyomark et al., 2010; Oskoei and Hu, 2006]

$$MAV = \frac{1}{N}\sum_{k=1}^{N}|x_k| \tag{7.1}$$

where x_k is the value of the k'th sample and N is the number of samples in the window.

Modified Mean Absolute Value (MMAV)

To improve the robustness of the MAV feature, a modified version has been proposed, where the data is smoothed by a Hanning window function. MMAV is defined as: [Phinyomark et al., 2010]

$$MMAV = \frac{1}{N}\sum_{k=1}^{N} w_k|x_k| \tag{7.2}$$

where x_k is the k'th sample of the EMG, w_k is the k'th sample of the Hanning window and N is the number of samples in the window.

Mean Absolute Value Slope (MAVSLP)

MAVSLP is another modified version of the MAV feature. MAVSLP is the difference between adjacent MAV values and can thus be used as an estimate for the amount of change in the amplitude of the EMG signal. It is defined as: [Phinyomark et al., 2010; Oskoei and Hu, 2006]

$$MAVSLP = MAV_{i+1} - MAV_i, \quad \text{for } i = 1, ..., I-1 \tag{7.3}$$

where i is i'th window and I is the total number of windows.

Root Mean Square (RMS)

RMS is used as an estimate of the standard deviation of the signal representing the power content. It is defined as: [Phinyomark et al., 2010; Oskoei and Hu, 2006]

$$RMS = \sqrt{\frac{1}{N}\sum_{k=1}^{N} x_k^2} \tag{7.4}$$

where x_k denotes the k'th sample and N is the number of samples in the window.

Variance (VAR)

The variance is an estimate of the power content of the signal. It is defined as: [Phinyomark et al., 2010; Oskoei and Hu, 2006]

$$VAR = \frac{1}{N}\sum_{k=1}^{N} (x_k - \mu)^2 \tag{7.5}$$

where x_k is the k'th sample, N is the number of samples in the window and μ is the mean of these samples.

Waveform Length (WL)

WL is the cumulative length of the waveforms in the signal. The feature is therefore influenced by waveform frequency, amplitude and duration. It is defined as: [Phinyomark et al., 2010; Oskoei and Hu, 2006]

$$WL = \sum_{k=2}^{N} |x_k - x_{k-1}| \tag{7.6}$$

where x_k is the k'th sample and N is the total number of samples in the window.

Willison Amplitude (WAMP)

WAMP is a measure of motor unit activity while ignoring the influence of noise by applying a threshold. It is defined as: [Phinyomark et al., 2010; Oskoei and Hu, 2006]

$$WAMP = \sum_{k=1}^{N-1} f(|x_k - x_{k+1}|), \quad f(x) = \begin{cases} 1, & \text{if } x > \varepsilon \\ 0, & \text{otherwise.} \end{cases} \tag{7.7}$$

where k is the k'th sample, N is the total number of samples in the window and ε is the threshold. Thus, WAMP represents a count of amplitude differences larger than the threshold.

Zero Crossing (ZC)

ZC is an estimate of the frequency properties of the signal, while excluding the effect of noise through a threshold. It is defined as: [Phinyomark et al., 2010; Oskoei and Hu, 2006]

$$ZC = \sum_{k=2}^{N} f\left[(x_k - \varepsilon) \cdot (x_{k-1} - \varepsilon)\right], \quad f(x) = \begin{cases} 1, & \text{if } x < 0, \\ 0, & \text{otherwise.} \end{cases} \tag{7.8}$$

where k is the k'th sample, N is the total number of samples and ε is the threshold. Thus, ZC represents the number of times the EMG crosses the axis while minimizing the effect of noise.

Slope Sign Changes (SSC)

Similarly to ZC, SSC is a measure of the frequency characteristics of the signal, while excluding the effect of noise through a threshold. It is defined as: [Phinyomark et al., 2010; Oskoei and Hu, 2006]

$$SCC = \sum_{k=2}^{N-1} \left[f\left[(x_k - x_{k-1}) \cdot (x_k - x_{k+1})\right]\right] \quad f(x) = \begin{cases} 1, & \text{if } x \geq \varepsilon, \\ 0, & \text{otherwise.} \end{cases} \tag{7.9}$$

where k is the k'th sample, N is the total number of samples in the window and ε is the threshold. Thus, SSC is the number of changes in the slope of the signal.

Calculation of the used thresholds

As mentioned, the three features WAMP, ZC and SSC require thresholds to ignore the effect of noise. To optimize these thresholds, an algorithm was developed, which automatically determined the optimal thresholds for each subject.
In the algorithm, the threshold was varied from a very low value, preserving the entire signal and much noise, to a very high value minimizing noise but also removing signal components. The optimization parameter was chosen as the difference between feature values during the rest period (noise) and active period (signal) of each profile - referred to as signal noise difference (SN).
The outcome of this can be seen in figure 7.1, where the threshold was set according

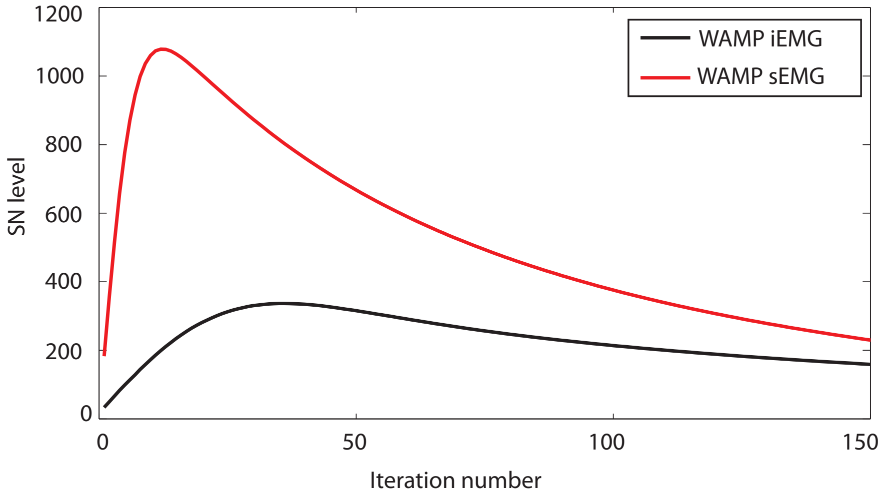

Figure 7.1: Example of the value of SN at different iterations for the WAMP feature for one subject.

to the global maximum of the optimization parameter SN.
The algorithm worked as follows for both sEMG and iEMG

1. Initialize thresholds as a very low value (empirically determined)
2. Calculate the average feature value at rest (N) (first 3 s of each profile) based on all 8 profiles and all 6 channels.

$$N = \frac{\sum_{chan=1}^{6} n_{chan} + \sum_{prof=1}^{8} n_{prof}}{6 \cdot 8}$$

3. Calculate the average feature value over a long period of activity (S), i.e., while performing several e.g. flexion movements, based on all 8 profiles and all 6 channels.

$$S = \frac{\sum_{chan=1}^{6} s_{chan} + \sum_{prof=1}^{8} s_{prof}}{6 \cdot 8}$$

4. Calculate and save SN (signal-noise) $SN = S - N$.
5. Increment threshold.
6. Recalculate step 1-5
7. Find and save the threshold corresponding to the global maximum of SN.

7.2.2 Frequency-domain features (FD)

The FD features were calculated according to the formulas given below.

Mean Power (MP)

The mean power of the PSD is a direct measure of the power in the signal. It is defined as: [Phinyomark et al., 2012]

$$MP = \frac{1}{M} \sum_{j=1}^{M} P_j \tag{7.10}$$

where P_j is the power of the j'th frequency and M is the total number of frequencies.

Auto-regressive model (AR)

The AR model describes the EMG signal through P previous samples, where P is the model's order. It is defined as: [Phinyomark et al., 2010; Oskoei and Hu, 2006]

$$x_i = \sum_{p=1}^{P} (a_p x_{i-p} + w_i) \tag{7.11}$$

where x_i is the i'th sample of the signal, a_p is the p'th AR-model coefficient and w_i is the i'th error term of white driving noise. The coefficients a are estimated using the Yule-Walker approach for a model of order six. This yields seven coefficients, where the first coefficient is always 1, and thus the remaining six coefficients were used as six features.

7.2.3 Time-frequency domain features (TFD)

TFD features were calculated based on the STFT and WT as described below.

Center of Mass (CoM)

CoM was calculated based on a STFT of the EMG signal within a given window. The STFT was calculated by dividing the window into eight segments using a Hamming

window with 50 % overlap between each segment, and for each segment calculate the PSD.
CoM can be used to represent the many values of the STFT. The feature was used to represent the change in position of the CoM on the frequency axis. It is defined as: [Farina et al., 2008]

$$CoM = \frac{1}{M}\sum_{l=1}^{N} m_l \vec{p}_l \tag{7.12}$$

where M is the total mass, m_l and p_l is the mass and position of the l'th sample of the STFT and N is the total number of samples in the STFT.

Discrete Wavelet Transform (DWT)

For each window, the DWT was calculated using a quadrature mirror filter composed of a low-pass and a high-pass filter determined by the used mother wavelet. The signal was convolved with the low-pass filter providing the 1st level approximation coefficients (cA1) and, simultaneously, convolved with the high-pass filter providing the detail coefficients (cD1), see figure 7.2. To increase the resolution in frequency, the same procedure was used on cA1, providing cA2 and cD2 and so on. For each level, the maximum frequency content in the signal was downscaled by a factor 2 (dyadic decimation).
Since sEMG and iEMG have different signal characteristics and frequency bands, it is reasonable to use different mother wavelets and decomposition levels. It was chosen to use daubechies 2 for sEMG and coiflet 5 for iEMG with decomposition levels of 4 and 3, respectively, based on the literature and on the similarity between these mother wavelets and the EMG signals. Phinyomark et al.; Khezri and Jahed; Englehart et al.

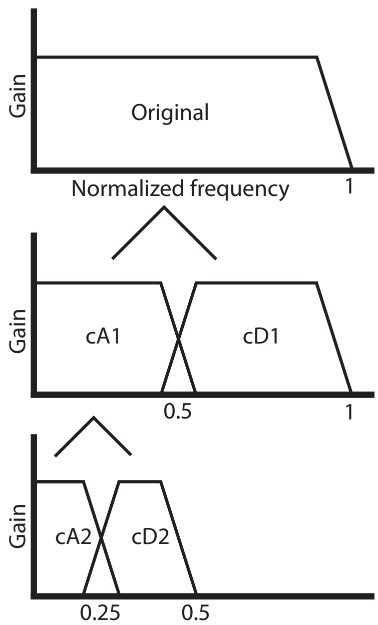

Figure 7.2: Decomposition of the signal into approximation (cA) and detail (cD) coefficients using filter banks.

DWTMAV

As a feature for each decomposition level, MAV (as described in eq. 7.1) was calculated. MAV was calculated for cDs at each level, and both cA and cD at the final level; i.e., five MAV values (cD1-cD4 and cA4) for sEMG and four values (cD1-cD3 and cA3) for iEMG. [Phinyomark et al., 2011]

DWTRMS

Similarly to DWTMAV, RMS values (as described in eq. 7.4) were calculated using the same approach. [Phinyomark et al., 2011]

7.3 Dimensionality Reduction

For each of the calculated features, each channel of EMG provided at least one dimension (known as a variable) in the feature space. The features CoM, MP and each TD feature provided 1 variable per channel, the AR feature provided 6 variables per channel, and DWTMAV and DWTRMS features provided 5 and 4 variables per channel for sEMG and iEMG, respectively. Thus, if all features were combined, the feature space would have 162 and 150 variables for sEMG and iEMG, respectively. To reduce the complexity of the feature space, and thereby avoid the curse of dimensionality, the two dimensionality reduction techniques SEPCOR and PCA were implemented.

Separability and Correlation (SEPCOR)

The SEPCOR algorithm treats discriminative power as information, and thus selects the variables, which best discriminates groups in the data. The algorithm is based on the value V calculated by eq. 7.13 [Ege et al., 2000]

$$\vec{V}_m = \frac{\text{The variance of the average values in } x_m}{\text{The average value of the variances in } x_m} \tag{7.13}$$

where x_m is the m'th variable.

After calculating the V-values, the algorithm consisted of two steps. First, all V-values below a threshold set to 0.2 were removed. Next, three simple steps were performed: [Ege et al., 2000]

1. Remove and save the variable with highest V_m
2. Find the correlation between the removed and the remaining variables
3. Remove variables with a maximum correlation higher than a given threshold

These steps were performed until all variables were either saved (i.e., step 1) or removed (i.e., step 3). [Ege et al., 2000]

Principal Component Analysis (PCA)

Contrary to SEPCOR, the PCA algorithm treats variance as information where a predefined variance of the feature space is retained using as few variables as possible.

The algorithm consists of 7 steps for a D-dimensional feature space: [Duda et al., 2000]

- Compute a mean vector of D-dimensions (a mean value for each variable)
- Compute a covariance matrix of the feature space of D×D-dimensions
- Compute the eigenvalues and -vectors of the covariance matrix
- Sort eigenvalues and -vectors according to eigenvalue in descending order
- Calculate the cumulative variance (power) described by the eigenvalues
- Select the number of eigenvalues necessary to describe the minimum variance desired
- Transform the original data using a matrix of the eigenvectors corresponding to the chosen eigenvalues.

By applying these steps, the data was transformed to fewer variables equal to the number of chosen eigenvalues. [Duda et al., 2000]

7.4 Classification

In order to classify movements based on the EMG signal, a classifier was needed. However, to train and test the classifier, it was necessary to know exactly when the subject performed a movement and which movement it was. Therefore, the data had to be labeled.

7.4.1 Labeling of data

The labeling of movements was done manually by identifying when the torque curve crossed the x-axis. As shown in the upper plot on figure 7.3, only one torque channel was active representing a single DoF, e.g. flexion/extension. If the movement consisted of 2 DoFs, two torque channels were active. However, commonly the two lines crossed the x-axis at slightly different time due to imperfect execution of the movements, as seen on the lower plot on figure 7.3. In such cases, the transition was identified at the center of the two lines. This constitutes a compromise between favoring the crossing of each of the two movements.

7.4.2 Linear Discriminant Analysis (LDA)

Many algorithms have been used to perform an LDA, which are distinguished by the number of discriminant analyses needed. To avoid ambiguous regions, i.e., regions in the feature space not belonging to a class, the approach used implemented c discriminant analyses (one for each class) defined as: [Duda et al., 2000]

$$g_i(x) = -\frac{1}{2}\,(\vec{x}-\vec{\mu}_i)^t\,\Sigma_p^{-1}\,(\vec{x}-\vec{\mu}_i) - \frac{d}{2}\ln(2\pi) - \frac{1}{2}\ln(\det(\Sigma_p)) + \ln P(\omega_i) \quad (7.14)$$

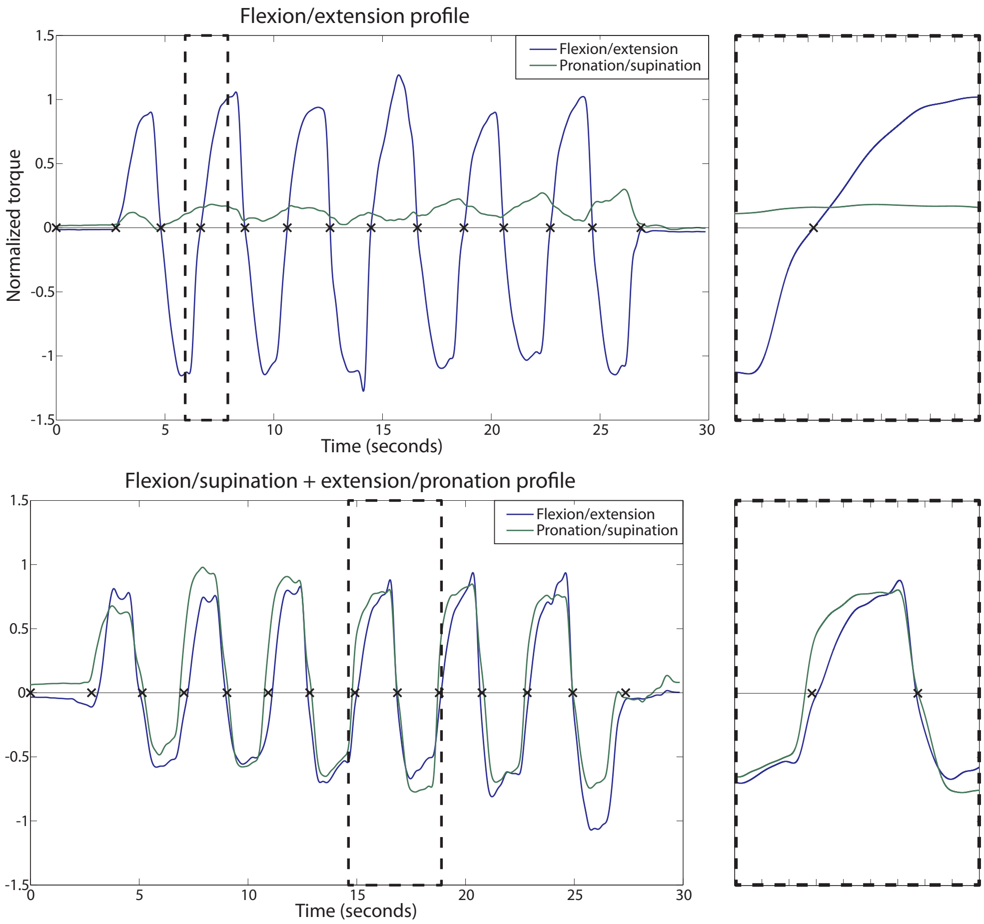

Figure 7.3: Example of labeled data, where the crosses indicate a transition between movements. The upper plot shows the trivial procedure of placing these on a single DoF profile (flexion/extension depicted). The lower plot shows the trade-off necessary to mark the changes on a two DoF profile (flexion/supination + extension/pronation depicted)

where $\vec{x}$ is the observation, $\vec{\mu}_i$ is the mean vector of the i'th class given by 7.16, Σ_p is the pooled covariance matrix with elements given by eq. 7.17, d is the number of dimensions and $P(\omega_i)$ is the a priori probability of the i'th class.
Since $(d/2)ln(2\pi)$ and $(1/2)ln(det(\Sigma_p))$ are independent of i, these are additive constants, which therefore were ignored. Moreover, since the a priori probability was the same for all classes, and thus uniformly distributed, this could also be treated as a superfluous constant and removed. Lastly, by expanding the quadratic form $(\vec{x}-\vec{\mu}_i)^t\Sigma_p^{-1}(\vec{x}-\vec{\mu}_i)$, a quadratic term $\vec{x}\,^t\Sigma_p^{-1}\vec{x}$ appears as a summed term independent of i, and thus the equation for the LDA was simplified to:

$$g_i(x) \quad = \quad (\Sigma_p^{-1}\,\vec{\mu}_i)^t\,\vec{x} - \frac{1}{2}\vec{\mu}_i^{\,t}\,\Sigma_p^{-1}\,\vec{\mu}_i \tag{7.15}$$

where the elements of the mean vector $\vec{\mu}_i$ for the i'th class are given by:

$$\mu_k \quad = \quad \frac{1}{N_i}\sum_{n=1}^{N_i} x_{kn} \quad \text{for } k = 1,2,..,V \tag{7.16}$$

where k is the k'th variable, n is the n'th observation, N_i is the number of observation in the i'th class and V is the total number of variables. The elements of the pooled covariance matrix are given by:

$$\Sigma_{jk} \quad = \quad \frac{1}{N_t - 1} \sum_{n=1}^{N_t} (\, x_{nj} - \mu_j \,)\,(\, x_{nk} - \mu_k \,) \tag{7.17}$$

where j is j'th variable, μ_j is the global mean of the j'th variable (disregarding the class), μ_k is the global mean of the k'th variable and N_t is the global number of observations.

A new observation was classified based on the value of g for all the classes, where the class i corresponding to the largest value of g was chosen. That is, assign x_n to class ω_i if $g_i(x_n) > g_j(x_n)$ for all $j \neq i$. Theoretically, in case of a tie, i.e., $g_i(x_n) = g_j(x_n)$ for $j \neq i$, the observation was disregarded.

7.4.3 k Nearest Neighbor (kNN)

kNN is a relatively simple classifier, which classifies a new observation based on the k nearest observations in the training data. The method utilizes a Euclidean distance measure, see eq. 7.18, and selects the most frequent class of the k nearest observations in the training data. [Duda et al., 2000]

$$Dist(a,b) \quad = \quad \sqrt{\sum_{i=1}^{D} (a_i - b_i)^2} \tag{7.18}$$

The value of k was set to 5 to avoid classification based on too few observations while keeping the pick-up area localized. In case of two classes being represented with the highest and equal frequency, it was chosen to classify the new observation based on the class of the former observation.

7.4.4 Support Vector Machine (SVM)

SVM is a binary classifier that separates two classes using an optimal separating hyperplane. The optimal hyperplane is found by maximizing the distance from the hyperplane to the nearest training observation on both sides. This distance is referred to as the margin, see figure 7.4 a). Thus, the SVM is known as a maximum margin classifier. [Abe, 2010]

However, maximizing the margin in this way requires that training observation are linearly separable, which is often not the case. Therefore a soft margin can be introduced, which allows training observations to fall within the margin or be misclassified (soft margin SVM). However, observations that are located inside the margin or misclassified are given a penalty, see figure 7.4 b). Thus, in order to find the optimal

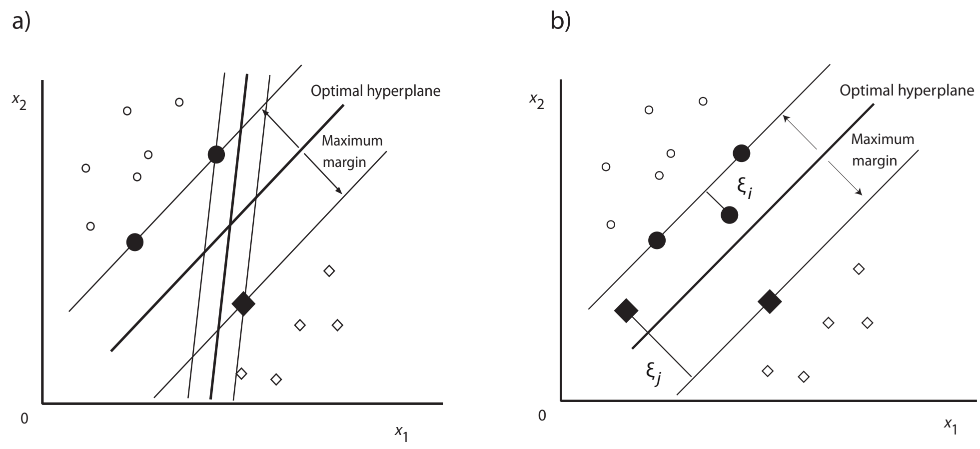

Figure 7.4: Determination of separating hyperplane and margins. a) margin if data is linearly separable, and b) soft margin approach where ξ represents the training observation penalty if it is within the margin or misclassified by the hyperplane. [Abe, 2010]

separating hyperplane the margin must be as wide as possible (by allowing training observations to fall within the margin or be misclassified) while still keeping the penalty as small as possible. [Abe, 2010]
Even though the separating hyperplane is determined in the optimal way, the SVM may still not be able to separate the data if it is not linearly separable. To overcome this problem, the SVM maps the training data into a higher dimension using a kernel where the data may be linearly separable. There are different kernel functions representing different mappings. The optimal kernel depends entirely on the nature of the data. As explained earlier, dimensionality reduction was used, which has a linearizing effect on the feature space and thus a linear kernel was used. [Englehart et al., 1999]
Since a SVM classifier is inherently binary, two methods was used to extend the functionality to allow classification of multiple classes. These are described below. [Abe, 2010]

One against all (SVMOAA)

In the one against all approach, the *n* classes were split into *n* two-class problems. For each problem a classifier was trained to distinguish between one class and the remaining classes (all). To classify a new observation, it was determined which class it belonged to with the *n* classifiers, i.e., where it did not belong to the all class. However, if the new observation was classified as none or more than one of the classes, it was unclassifiable. In such cases it was chosen to classify it as the previously classified observation. [Oskoei and Hu, 2006; Abe, 2010]

One against one (SVMOAO)

In the one against one approach, a classifier was trained for every pair of classes, thus C(C-1)/2 SVMs were trained. Each SVM determined whether a new observation belonged to one class or the other. This observation was classified by all the SVMs and assigned to the class with the highest frequency (the class most of the SVMs voted for). However, if two classes had the highest but equal number of votes, the observation was unclassifiable. In this case it was classified as the previously classified sample. [Oskoei and Hu, 2006; Abe, 2010]

7.4.5 Artificial Neural Network for movement classification

The ANN is an emulation of the biological neural network. The architecture of the network typically involves two layers; a hidden layer and an output layer [Beale et al., 2012].
In the hidden layer, the input data is, in parallel, multiplied with several weights (w^{hid}), summed and subtracted a bias (b^{hid}), see figure 7.5. Afterwards the data is passed through a transfer function (f^{hid}). As the first part of the output layer, the output from the neurons in the hidden layer (a) is weighted (w^{hid}), summed and subtracted a bias (b^{out}). This is passed through transfer functions (f^{out}) providing the network's output (y). [Beale et al., 2012]
The hidden layer consisted of 10 neurons ($S1$ = 10) and both transfer functions were

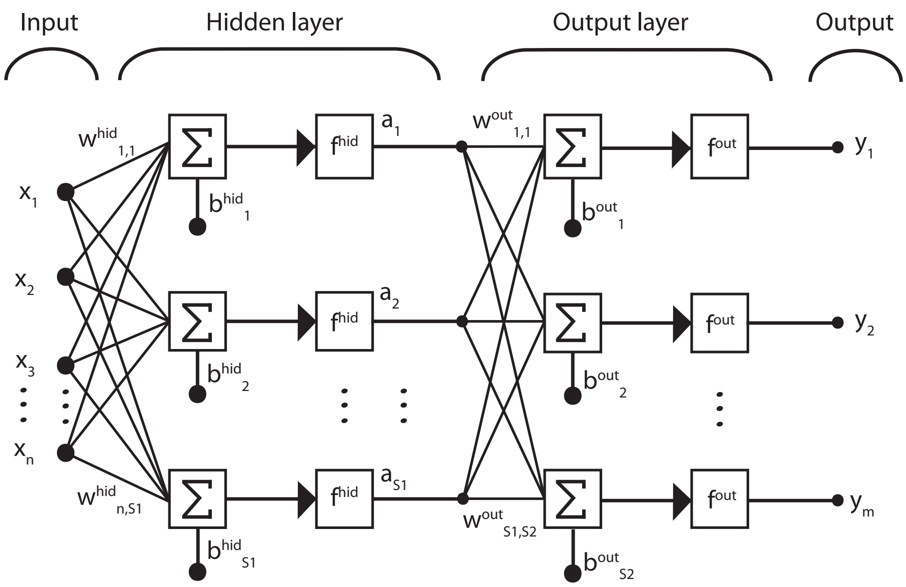

Figure 7.5: The design of a neural network with one hidden layer and one output layer. x_n is the n'th feature of the training data, w^{hid} and w^{out} are the individual weights of the hidden and output layer, respectively, b^{hid} and b^{out} are the biases, $S1$ and $S2$ are the number of neurons, f^{hid} and f^{out} are the transfer function, a is the output from the hidden layer and y_m is the output for the m'th class. [Beale et al., 2012]

chosen as hyperbolic tangent sigmoid functions. The number of neurons in the output layer ($S2$) was equal to the number of classes to predict.

To optimize the functionality of the network, it must be trained. This was done by providing the network with training data and the corresponding class labels. The training data was randomly divided into actual training data (70 %) and validation data (30 %), where the percentages describe the amount of data for each class. The network was then iteratively used to match the training data to the target class. This was done by updating the weights and biases in both layers to minimize the mean square error of the system. For each iteration, the validation data was used to avoid overfitting of the network, i.e., when the performance of the network on the validation data was worse than the performance in the previous iterations. [Beale et al., 2012]

To further optimize the performance of the network, a new network was created 50 times, where the above procedure was performed for each network. This was done to reinitialize all weights and biases as well as re-randomize the distribution of data to the training and validation data set. The performance of each network was assessed by using the network to predict the outcome of the entire training set and then calculate the percentage of correctly classified observations. The best of these 50 networks, determined by the highest classification accuracy on the training data, was then used to classify the new observations. [Beale et al., 2012]

7.4.6 Post processing

As post processing technique, MV was implemented. MV basically accumulate a number of results from the classifier and selects the class with the most occurrences. However, this also creates a delay in the system. Thus, before choosing the number of results for the MV, an acceptable delay in the system had to be specified. The delay created by the MV can be calculated as: [Farrell and Weir, 2008b]

$$D = \frac{1}{2}T_a + (\frac{n-1}{2})T_w + \tau \tag{7.19}$$

where T_a is the window length, T_w is the step size, n is the number of MVs and τ is the processing delay. Further, τ is set as zero since this parameter is only important in a real time implementation and should be very small. The formula can be isolated to return the number of votes for the MV given a certain allowed delay: [Farrell and Weir, 2008b]

$$n = \frac{2 \cdot D \; - \; T_a}{T_w} + 1 \tag{7.20}$$

In case of a tie between two or more classes the current observation was classified as the previously classified observation.

7.4.7 Outcome measures

The performance of the movement classification was determined as classification accuracy given by the formula: [Scheme and Englehart, 2011]

$$Acc = \frac{\text{Number of correct decisions}}{\text{Total number of decisions}} \cdot 100\% \tag{7.21}$$

7.5 Force estimation

In order to estimate the corresponding force to the movements based on the EMG signal, a force estimator was needed. Below is a description of the two techniques used.

7.5.1 Artificial Neural Network for force

The ANN used for force estimation had the same functionality as the network described for movement classification. However, to estimate a torque profile it was chosen to use a linear transfer function in the output layer. [Beale et al., 2012]
To quantify the performance of each of the 50 created networks, a multi-dimensional coefficient of determination (explained in the next section) was calculated for the predicted torque based on the training data compared to the real measured torque. The network providing the highest value was used for the new observations.

7.5.2 Linear Model (LM)

Two linear models were implemented using linear predictor functions estimating the unknown model parameters based on training data. The equation for the linear model can be written as: [Mathworks, 2012]

$$\vec{y} \quad = \quad X\vec{\beta} + \vec{\varepsilon} \tag{7.22}$$

where $\vec{y}$ is a vector of the true torque, X is a matrix of training data, $\vec{\beta}$ is a vector of model coefficients and $\vec{\varepsilon}$ is the noise. The estimation of the model coefficients was performed through minimization of the least square error. In one of the two models, the standard least square error was used (LMorg) and for the second, a more robust method was used which minimized the effect of outliers (LMrob). [Mathworks, 2012]

7.5.3 Outcome measures

To quantify the output from the force estimator, the coefficient of determination (R^2) was used. However, since two torque channels were predicted, the original

1-dimensional R^2-value could not be used. Thus, a multi-dimensional R^2 was implemented: [d'Avella et al., 2006]

$$R^2 = 1 - \frac{\sum_{i=1}^{D} SS_{err}(i)}{\sum_{i=1}^{D} SS_{tot}(i)} \tag{7.23}$$

where D is the number of dimensions, and SS_{err} and SS_{tot} are given by:

$$SS_{err} = \sum_{k}^{N} (y_k - f_k)^2 \tag{7.24}$$

$$SS_{tot} = \sum_{k}^{N} (y_k - \bar{y})^2 \tag{7.25}$$

where y_k is the k'th measured sample, f_k is the k'th estimated sample and $\bar{y}$ is the mean of the measured observations. The multi-dimensional R^2 is a relatively simple extension of the 1-dimensional R^2 given by: [Rosenvang et al., 2010a]

$$R^2 = 1 - \frac{SS_{err}}{SS_{tot}} \tag{7.26}$$

To mimic the outcome of a prosthesis, it was chosen to implement a one-dimensional R^2 as well. This value was calculated for each channel independently based on the result of the classifier. E.g., if the classifier determined flexion, the sample was estimated using the found relationship for that movement. The final R^2-value was then calculated as a weighted average between the outcome of the two single R^2-values (one for each torque channel).

7.6 Statistical analysis

To choose the statistical tests needed for the analysis, the distribution of the data was investigated. Through pilot experiments it was found that the outcome measures (classification accuracy and R^2) were not normally distributed, and thus nonparametric tests had to be used. To compare two groups of more than 30 observations, the paired t-test was used. To avoid type I errors through multiple pairwise comparisons, Friedman's two-way analysis of variance with adjusted post-hoc comparison was used for analysis on more than two groups. The two tests are explained below. [Mathworks, 2012; Corder and Foreman, 2009]

7.6.1 Paired t-test

The paired t-test is similar to a one-sample t-test, where the test sample is instead given by the difference between the two paired samples, i.e., x = sample one - sample two. The test statistic (t) for a paired t-test is therefore given by: [Zar, 2010]

$$t = \frac{\bar{x} - \mu}{s/\sqrt{n}} \tag{7.27}$$

where $\bar{x}$ is the sample mean, μ is the hypothesized mean, s is the sample standard deviation and n is the sample size. The test statistic, t, can be converted to a p-value through a table look-up. [Zar, 2010]

The hypothesis of the test was that the mean of x was zero. This hypothesis was rejected if the p value was below 0.05

7.6.2 Friedman's two-way analysis of variance

The test statistic (F_r) for a Friedman test is calculated on ranked sample data. It is given by: [Corder and Foreman, 2009]

$$F_r = \frac{12}{nk(k+1)} \sum_{i=1}^{k} R_i^2 - 3n(k+1) \tag{7.28}$$

where n is the number of samples, k is the number of groups and R_i is the sum of the ranks for group i. If any duplicate ranks are found, a correction is added. The test statistic, F_r, can be converted to a p-value through a table look-up. [Zar, 2010]

The hypothesis of the test was that the distributions of the samples are equal. This hypothesis was rejected if the p value was below 0.05, where a corrected pairwise comparison was performed between the groups.

Optimization and validation strategy 8

In the process of designing a hybrid control scheme, the components seen in figure 5.1 must be specified. Each of these components includes parameters, e.g. choice of features, which were further specified in the aim in figure 5.2. The optimal combination of these parameters must be found and later used for validation of the system.

8.1 Optimization of parameters

The parameters of the control scheme that could adjusted were:

- Features
- Window
- Filtering of features
- Dimensionality reduction method
- Movement classifier
- Post processing
- Force estimator

There exists thousands of combinations of the parameters mentioned above, which in practice was impossible to investigate due to time constraints. Therefore, a strategy was needed in order to investigate the performance of the control scheme when adjusting the different parameters. The approach was in general to investigate the effect of each step in the design process, find the parameters that provided the best results and maintain these parameters in the next step. For all steps, results from sEMG, iEMG and combined sEMG and iEMG (cEMG) were considered. The investigation was based on a four-fold cross-validation, where all profiles were split in half for the two trials. Thus, all 9 classes (8 movements + rest) were represented.

8.1.1 Step 1 - selection of optimal TD feature set

Pattern recognition

The purpose of step one was to determine the optimal choice of TD features for different window sizes.

To find the optimal TD feature combination, all feature subsets had to be considered, i.e. combining 1, 2 and up to all 9 features. The total number of possible combinations can be calculated using the formula:

$$K(n,P) = \sum_{P=1}^{n} \frac{n!}{P! \cdot (n-P)!} \tag{8.1}$$

where n is the total number of features (n = 9) and p is the number of features to be combined. The total number of feature combinations was thus 511.
In this step it was also chosen to investigate window sizes (50 ms, 100 ms, 150 ms, 200 ms, 300 ms, 400 ms and 500 ms) with a step size of 50 ms (overlapped windows). A step size of 50 ms was chosen to obtain more data points for classification compared to non-overlapping windows. Furthermore, the choice of step size should not affect accuracy if no post processing was performed.
To investigate seven windows, each with 511 feature combinations, a fast classifier was needed due to the time constraints of the project. Thus, it was chosen to use the LDA classifier, since this was the fastest among the possible choices (SVM, kNN, ANN) and, moreover, it has shown good performance throughout the literature.

For step 1-4, the following parameters were held constant: LDA classifier, PCA dimensionality reduction, fourth order Butterworth band-pass filter and no post processing.

Proportional control

In order to find the best performing features for force estimation, ideally the same approach for force estimation as in movement classification should be performed. However, the force estimator was based on ANN, which takes approximately 30 minutes for each feature combination. Thus, performing 3577 of such would take $\approx$ 75 days. Therefore, the chosen features for force estimation were based on the analysis from pattern recognition. Moreover, we believe that determining the correct movements is more important than finding the exact force level, since force will have no meaning if the movement is incorrect. This applies for all the steps, which optimize the control scheme performance, i.e. step 1-6.

8.1.2 Step 2 - selection of the optimal complete feature set

In step 2, the best performing TD feature set was combined with the other feature domains to find the overall best performing feature set. Specifically, the TD subset was combined with the FD features (AR, MNP), and the TFD feature (CoM, DWTRMS, DWTRMS) for all window sizes.
Thus, a total of three feature combinations for each window were investigated and compared to the TD feature set determined in step 1:

- TD + FD
- TD + TFD
- TD + FD + TFD

8.1.3 Step 3 - selection of optimal window length

During step 1 and 2, the best performing feature set was chosen. The purpose of step 3 was to investigate which window provided the best classification accuracy with the feature set found in step 2. Window sizes were investigated, since the length of the window impacts the performance of the control system and the delay of the control scheme. The delay is given by the formula below: [Farrell and Weir, 2008b]

$$D = \frac{1}{2}T_a + \tau \tag{8.2}$$

where T_a is the window length and τ is the processing delay of the system. The effect of τ was neglected, since its value should be based on the processing time of a control system implemented on a micro-processor in a myoelectric prosthesis. In general, the value should be as small as possible. [Farrell and Weir, 2008b]

8.1.4 Step 4 - selection of feature filtering

In step 4, the best performing feature set and window length was held constant, while investigating the effect of filtering the features. Filtering features provides a smoother feature set and may have an effect on classification accuracy across different classifiers. Furthermore, the impact of smoothing the features on classification accuracy has not been investigated before.

8.1.5 Step 5 - selection of dimensionality reduction method and classifier

In step 5, the effect of dimensionality reduction (PCA, SEPCOR) of the feature set was investigated across the different classifiers (LDA, kNN, ANN, SVMOAO, SVMOAA). Classifiers and dimensionality reduction methods were investigated together since the different classifiers may respond differently to the dimensionality reduction methods. Additionally, to compare the two methods, their parameters defining the minimum variance (PCA) and maximum correlation (SEPCOR) were adjusted using the values:

- PCA: Minimum variance = 0.95
- PCA: Minimum variance = 0.99
- PCA: Minimum variance = 0.999
- SEPCOR: Maximum correlation = 0.8
- SEPCOR: Maximum correlation = 0.9
- SEPCOR: Maximum correlation = 0.95

The results from step 5 were used to determine the last parameters, which were the dimensionality reduction method and its parameters, and the classifier with the best performance.

8.1.6 Step 6 - selection of post processing parameters

In step 6, the effect of post-processing (MV) was investigated. For a given acceptable delay of the system, a different number of samples could be used for the MV. It was chosen to investigate windows of 50, 100 and 150 ms at step sizes equal to 25, 50, 100 and 150 ms with an acceptable delay of 200 ms.
The following combinations of windows and steps were used to calculate the number of MVs using formula 7.20 and are given in table 8.1.

Window [ms]	**Step [ms]**	**n [number of MVs]**
50	25 and 50	15 and 8
100	25, 50 and 100	13, 7 and 4
150	25, 50, 100 and 150	11, 6, 3 and 2

Table 8.1: Number of samples for the MV according to an acceptable delay of 200 ms at different window and step sizes.

Furthermore, the effect of post-processing was compared to a window of 400 ms, which induced an equal acceptable delay without using post-processing, calculated by formula 8.2.

8.1.7 Step 7 - selection of force estimator

In step 7, the effect of different force estimators was investigated (LMorg, LMrob and ANN). This was done to choose the force estimator giving the highest R^2 considering both the one and two dimensional R^2.

8.2 Validation of system

A nine class problem (all possible classes) with four fold validation was used, while finding the optimal parameters for the myoelectric control scheme. However, the control scheme was also validated for movement classification and force estimation to compare how the signals (iEMG, sEMG and cEMG) performed individually.

8.2.1 Step 1 - evaluation of number of classes

In step 1 of the validation, it was assessed how the number of included classes affected movement classification and force estimation. This was done by excluding some of the classes from the used data, representing a more simple problem for the control system. Classes were divided into single movements and simultaneous movements in the following way:

1. 3 classes: Flexion and extension
2. 3 classes: Pronation and supination

3. 3 classes: Flexion+pronation and extension+supination
4. 3 classes: Flexion+supination and extension+pronation
5. 5 classes: Flexion, extension, pronation and supination
6. 5 classes: Flexion+pronation, extension+supination, flexion+supination and extension+pronation
7. 9 classes: all classes from the above

8.2.2 Step 2 - evaluation of modulated profile

In step 2 of the validation, the outcome of using the modulated profile as test data while training on trial one and two (normal profiles) was investigated. The modulated profile corresponded to doing the same movements as in trial one and two with varying amplitude and frequency. This may resemble the real life case more, where the prosthesis is trained on data that is different from the data acquired during the day.

8.2.3 Step 3 - evaluation of mis-classifications

The data was dynamic in nature with 11 switches between movements for each performed profile, e.g. between flexion and extension. This resulted in periods of transition between two classes with almost zero force, which may pose difficulties for the classifier. Thus, the outcome of ignoring these transition periods was tested. The classifier and force estimator was trained using the whole data set, but the classification accuracy was calculated while ignoring the transition states. It was chosen to investigate different ignore zones determined as 0.05 - 0.25 seconds on either side of a transition in increments of 0.05 seconds. This ignore zone represented 7.9 % - 38.3 % of the targeted force level.

Results 9

In the previous chapter, the strategy for optimizing and validating the system was outlined. In this chapter, the results of these steps will be presented.
All results are based on a four-fold validation using PCA with an explained variance of 99 % unless otherwise stated.

9.1 Effect of different combinations of TD features

Using the cEMG with a window of 150 ms, 8 features provided the highest mean classification accuracy (cEMG: 85.8 % $\pm$ 4.6 % (mean$\pm$SD)), see figure 9.1. Similarly for sEMG and iEMG, the highest mean classification accuracy (sEMG: 81.9 % $\pm$ 4.4 %, iEMG: 74.9 % $\pm$ 6.7 %) was achived using 9 features for both signals.
In general for cEMG across all windows (50 ms, 100 ms, 150 ms, 200 ms, 300 ms, 400 ms, 500 ms), using 8 features resulted in the highest mean accuracy, although using more than 6 features did not provide any significant improvement ($p > 0.05$).

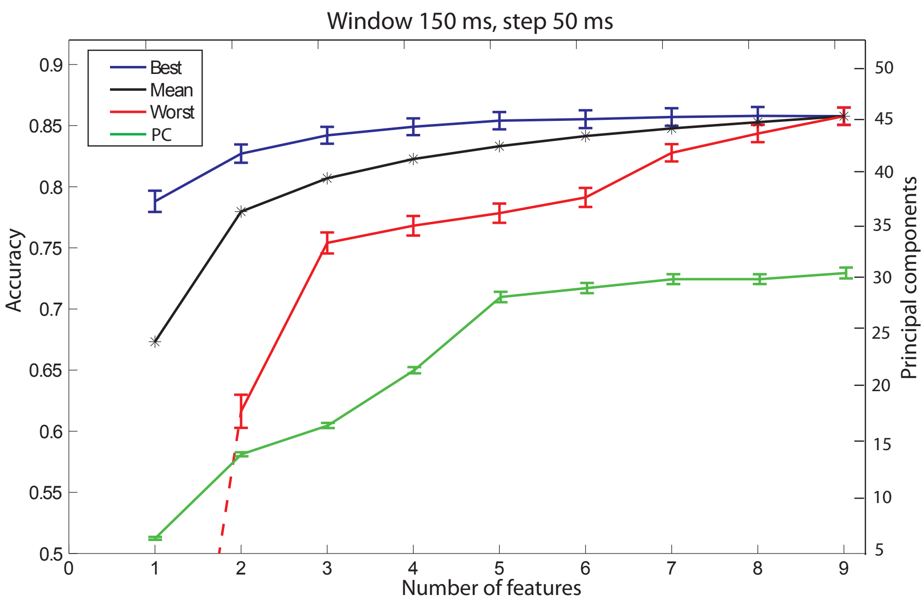

Figure 9.1: Classification accuracy when using a combination of 1 to 9 features for a 150 ms window using a step size of 50 ms for the cEMG signal across subjects. Mean refers to the mean performance of all different combinations of a feature subset. Best and worst refers to the best and worst performing feature subset, respectively. PC is the number of principal components used (axis to the right) according to the number of included features.

In general for sEMG and iEMG, the highest mean accuracies across all windows were achieved using 8 and 7 features, respectively. However, no significant increase in classification accuracy was found using more than 6 and 4 features, respectively ($p > 0.05$). The number of principal components used increased when adding more features, as shown in figure 9.1.
In general, no improvement was seen when adding *var* as a ninth feature for any of the signals or windows.
In the remaining of the results, *var* ***was removed from the TD feature set.***

9.2 Effect of different feature domains

The mean accuracies of using features from the different domains to TD features (excluding *var*) can be seen in figure 9.2 for the three signals with a window of 150 ms.

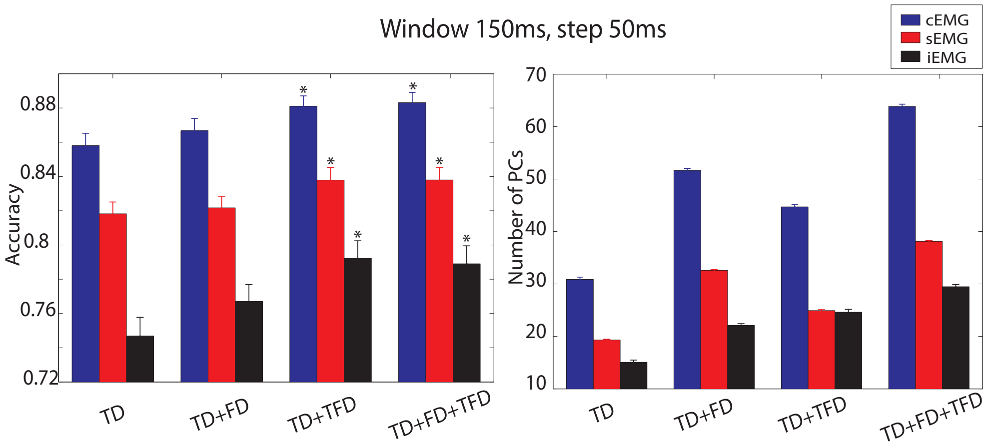

Figure 9.2: Classification accuracy (left) and corresponding number of principal components (right) according to different feature domains for the three EMG signals using a window of 150 ms with step size 50 ms. Stars (*) indicate highest significant classification accuracies achieved.

For this window, cEMG and sEMG provided the highest mean accuracy using all feature domains (cEMG: 88.3 % ± 3.8 %, sEMG: 83.8 % ± 4.6 %), whereas for iEMG this was achieved using the two features domains $TD + TFD$ (iEMG: 79.2 % ± 6.5 %). Similar results were observed for the remaining windows, albeit the highest mean accuracy for iEMG using longer windows (> 300 ms) was achieved using all domains.
Statistically, a significant difference was found between all feature domains across all windows ($p < 0.05$) except for adding FD to $TD + TFD$ ($p > 0.05$). The used principal components are shown in figure 9.2.
In the remaining of the results, all feature domains were used $(TD + FD + TFD)$**.**

9.3 Effect of different windows

Using all domains, the effect of different windows can be seen in figure 9.3. For all signals, the highest mean accuracy was achieved using the longest window of 500 ms. In general, the longer window used, a statistically higher mean accuracy was achieved ($p < 0.05$), although no improvement was found using longer windows than 400 ms for cEMG and iEMG, and 300 ms for sEMG ($p > 0.05$).
In the remaining of the results, a window of 150 ms with a step of 50 ms was used, unless otherwise stated.

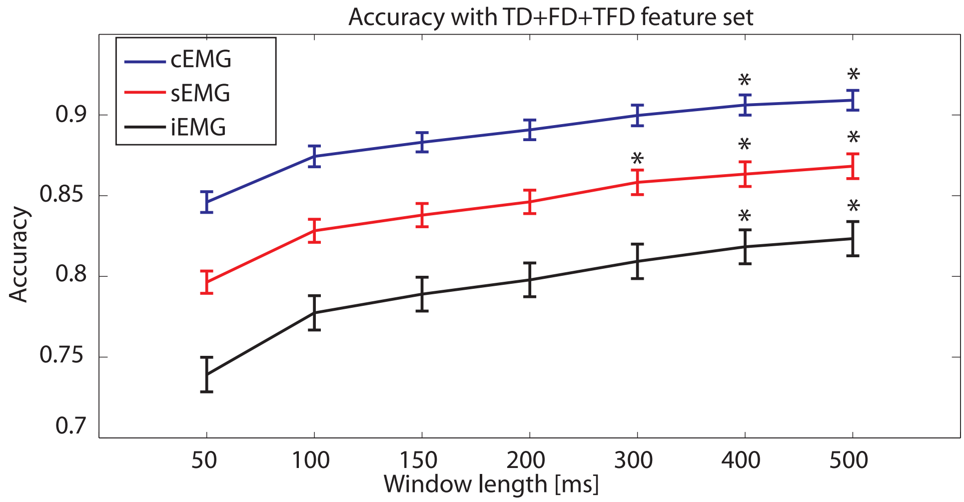

Figure 9.3: Classification accuracy for different window sizes with a step of 50 ms for the three signals. Stars (*) indicate highest significant classification accuracies achieved.

9.4 Effect of filtering features

The effect of applying a low-pass filter to the features is shown in figure 9.4. In general across signals, kNN and LDA showed a significant increase in classification accuracy ($p < 0.05$), ANN did not show any significant differences ($p > 0.05$) and the SVM classifiers showed a decrease, although only significant for cEMG with SVMOAA ($p < 0.05$), see table 9.1.
In the remaining of the results, all features were filtered.

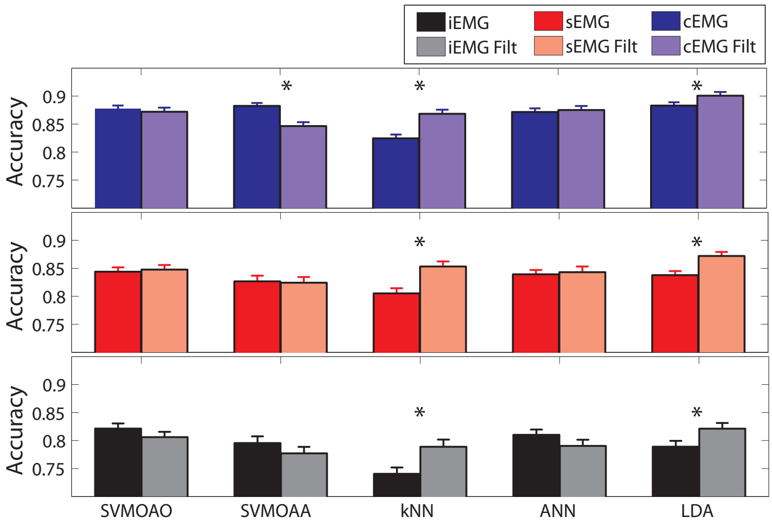

Figure 9.4: Classification accuracy for different classifiers with filtered or unfiltered features for the three signals. Stars (*) indicate significant difference between using filtered and unfiltered features.

	SVMOAO	SVMOAA	kNN	ANN	LDA
cEMG	-0.5 %	-3.6 %*	4.4 %*	0.3 %	1.8 %*
sEMG	0.4 %	-0.2 %	4.8 %*	0.4 %	3.4 %*
iEMG	-1.5 %	-1.8 %	4.8 %*	-2.0 %	3.2 %*

Table 9.1: Difference in classification accuracy between filtered and unfiltered features for the five classifiers. Negative numbers represents a drop in classification accuracy from filtering of the features. Positive numbers represent an increase in classification accuracy. * $p < 0.05$

9.5 Effect of classifier and dimensionality reduction method

The effect of applying different dimensionality reduction techniques (PCA and SEPCOR with different parameters) in relation to different classifiers can be seen in figure 9.5. In general for SEPCOR, increasing the maximum allowed correlation increased the amount of used variables, see table 9.2. In general, this also resulted in increased classification accuracy, as seen in table 9.3, however, only in some cases significantly.

	P95	P99	P99.9	S80	S90	S95
cEMG	13.5 ± 0.7	30.4 ± 1.5	76.4 ± 3.0	42.4 ± 3.5	60.0 ± 3.8	81.3 ± 3.7
sEMG	10.4 ± 0.6	21.1 ± 1.5	45.2 ± 1.8	23.2 ± 2.5	32.7 ± 3.1	44.9 ± 3.6
iEMG	11.9 ± 1.1	22.5 ± 1.2	46.6 ± 3.0	29.0 ± 2.4	38.8 ± 3.2	52.6 ± 4.5

Table 9.2: The number of variables used for the two dimensionality reduction methods (P: PCA, S: SEPCOR) with the three parameters (maximum correlation allowed and minimum amount of explained variance). The number of variables before dimensionality reduction was: 300 for cEMG, 156 for sEMG, and 144 for iEMG

For PCA, an increase in the number of used variables was seen when increasing the explained variance as seen in table 9.2. Mean classification accuracy also increased when the explained variance was increased from 95 % to 99 % as seen in table 9.3. However, increasing the explained variance further to 99.9 % did not consistently increase the accuracy further; on the contrary, a tendency towards a drop in mean accuracy was seen for both SVM classifiers for all signals and for ANN using cEMG.

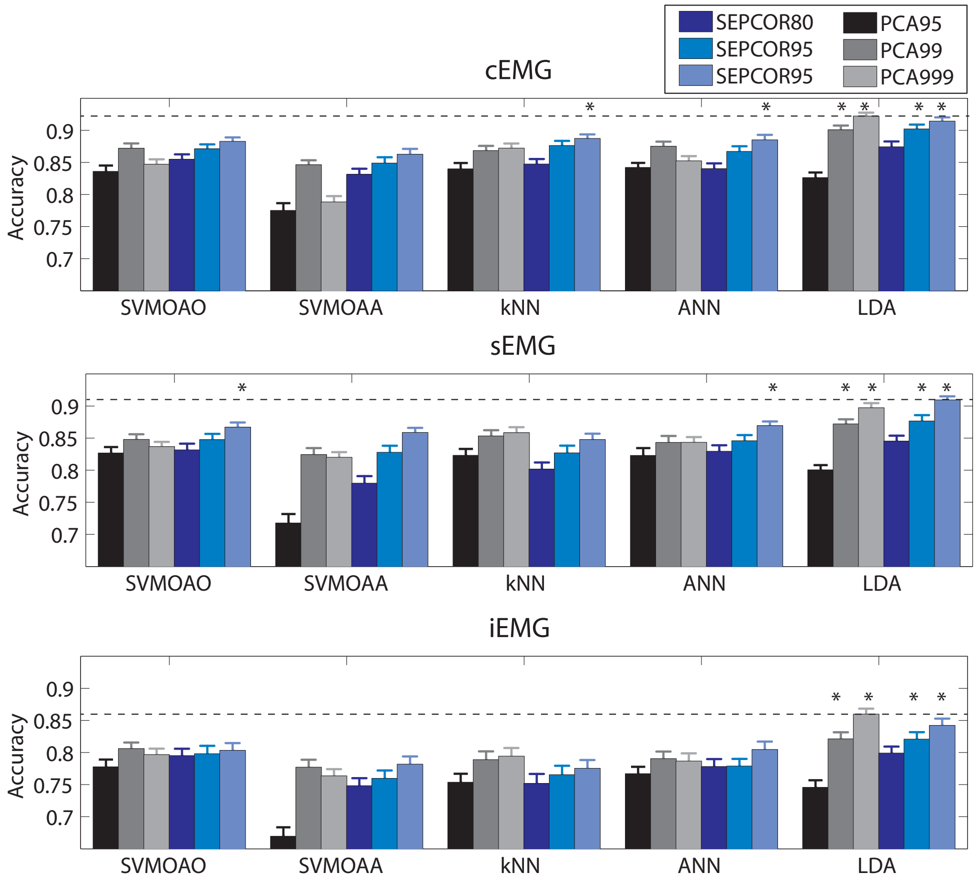

Figure 9.5: Classification accuracy for all classifiers using the two dimensionality reduction methods (each with three parameters) for all three signals. Stars (*) indicate significant highest classification accuracies achieved.

As seen in table 9.3 and figure 9.5, amongst the used classifiers, LDA benefits the most from increasing the amount of variables used; especially by increasing the number of principal components for the PCA.

For cEMG, LDA with PCA 99.9 % had a mean accuracy of 92.2 % ± 3.3 % significantly higher than all other classifiers with the different dimensionality reduction methods ($p < 0.05$) except kNN and ANN with SEPCOR95 ($p > 0.05$).
Similarly, for cEMG and LDA with SEPCOR95, a mean accuracy of 91.4 % ± 3.6 % was achieved significantly higher than all other classifiers ($p < 0.05$) except SVMOAO, kNN and ANN with SEPCOR95 ($p > 0.05$).

For sEMG, LDA with PCA 99.9 % had a mean accuracy of 89.7 % ± 4.5 % significantly different to all other classifiers ($p < 0.05$) except SVMOAO and ANN with SEPCOR95 and kNN with PCA 99.9 % ($p > 0.05$).
Similarly, for sEMG and LDA with SEPCOR95, a mean of 91.0 % ± 3.5 % was achieved significantly different to all other classifiers ($p < 0.05$) except SVMOAO and ANN with SEPCOR95 ($p > 0.05$).

For iEMG, LDA with PCA 99.9 % had a mean accuracy of 86.0 % ± 5.4 % was found significantly different from all other classifiers ($p < 0.05$).
Similarly, for iEMG and LDA with SEPCOR95, a mean accuracy of 84.22 % ± 6.7 % was achieved significantly higher than all other classifiers ($p < 0.05$) except SVMOAO with PCA 99 % and ANN with SEPCOR95 ($p > 0.05$).
In the remaining of the results, PCA 99.9 % was used with an LDA classifier.

	cEMG [%]				sEMG [%]				iEMG [%]			
	P99	**P99.9**	**S90**	**S95**	**P99**	**P99.9**	**S90**	**S95**	**P99**	**P99.9**	**S90**	**S95**
SVMOAO	3.6	1.1	1.6	2.8	2.1	1.0	1.6	3.5	2.8	1.9	0.3	0.8
SVMOAA	7.1*	1.3	1.8	3.1	10.7*	10.2*	4.8*	7.9*	10.8*	9.4*	1.1	3.3
kNN	2.8	3.2	2.9	4.0*	3.0	3.5	2.5	4.6*	3.5	4.1*	1.4	2.4
ANN	3.3*	1.0	2.7	4.5*	2.0	2.0	1.6	4.0	2.3	2.0	0.1	2.7
LDA	7.4*	9.6*	2.8	4*	7.2*	9.7*	3.1	6.4*	7.6*	11.4*	2.2	4.3*

Table 9.3: Difference in classification accuracy for the different classifiers, signals and dimensionality reduction methods. Positive numbers represent an increase in classification accuracy. * $p < 0.05$
P99 refers to the difference between PCA95 and PCA99.
P99.9 refers to the difference between PCA95 and PCA99.9.
S90 refers to the difference between SEPCOR80 and SEPCOR90.
S95 refers to the difference between SEPCOR80 and SEPCOR95.

9.6 Effect of post-processing

The effect of applying MVs allowing a delay in the control system of approximately 200 ms is shown in figure 9.6 for different window and step sizes. For comparison, classification accuracy for a window of 400 ms is shown as the horizontal line in figure 9.6. In general, the highest mean accuracy was achieved using the 400 ms window, although only significantly higher than W150S100 (window of length 150 ms with step size of 100 ms) for cEMG and W150S50, W150S100 and W150S150 for sEMG ($p < 0.05$). No significant differences were found for iEMG. In general, a shorter step-size and thus more MVs provided higher mean accuracies than longer step-sizes with fewer MVs.

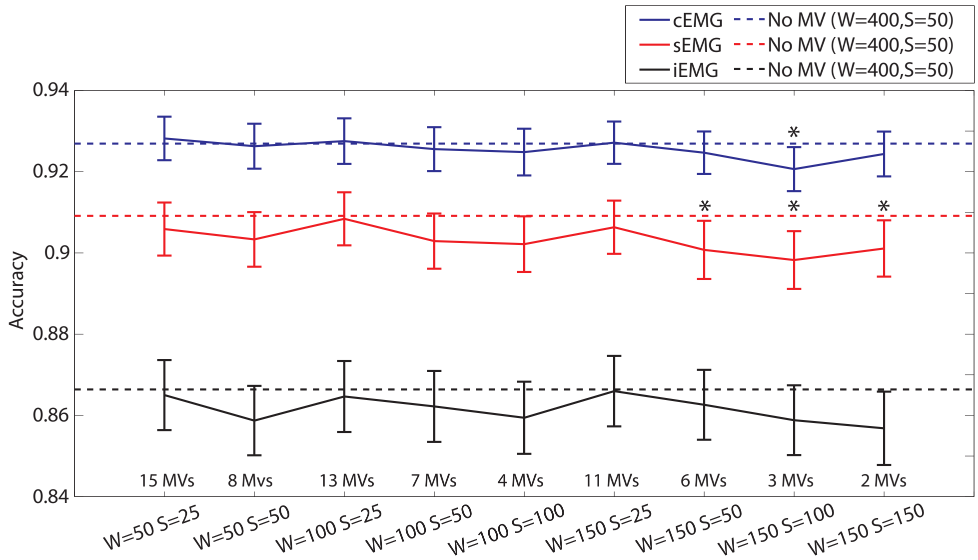

Figure 9.6: Classification accuracy when applying MVs for different window- and step-sizes tolerating a delay in the control system of approximately 200 ms. Stars (*) indicate significantly lower classification accuracies compared to a 400 ms window.

9.7 Effect of force estimator

The effect of applying different force estimators for the three signals can be seen in figure 9.7. For the one-dimensional R^2, no significant differences were found between the different force estimators for each signal ($p > 0.05$). For the two-dimensional R^2, the LM performed significantly better than the ANN for cEMG ($p < 0.05$). No other significant differences were found for sEMG and iEMG for the two-dimensional R^2. In general, the one dimensional R^2 showed higher accuracies compared to the two dimensional.

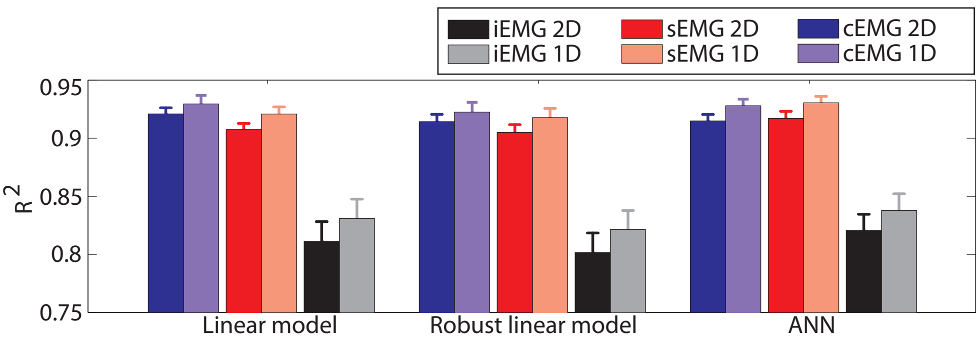

Figure 9.7: One- and two-dimensional R^2 for the different force estimators and signals.

An example of measured and estimated force during movements can be seen on figure 9.8 using the LM estimator.

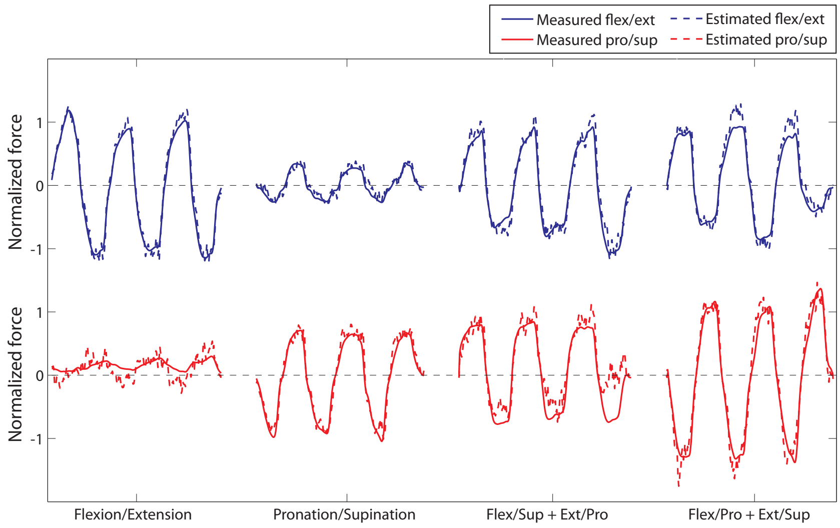

Figure 9.8: Measured and estimated force during movements using the LM estimator.

In the remaining of the results, LM was used as the force estimator.

9.8 Validation of control system

The outcome of the control system with all feature domains using PCA99.9 for LDA and LM can be seen in figure 9.10 for seven class combinations. Furthermore, the performance of each individual subject for the 9 class problem can be seen in figure 9.9

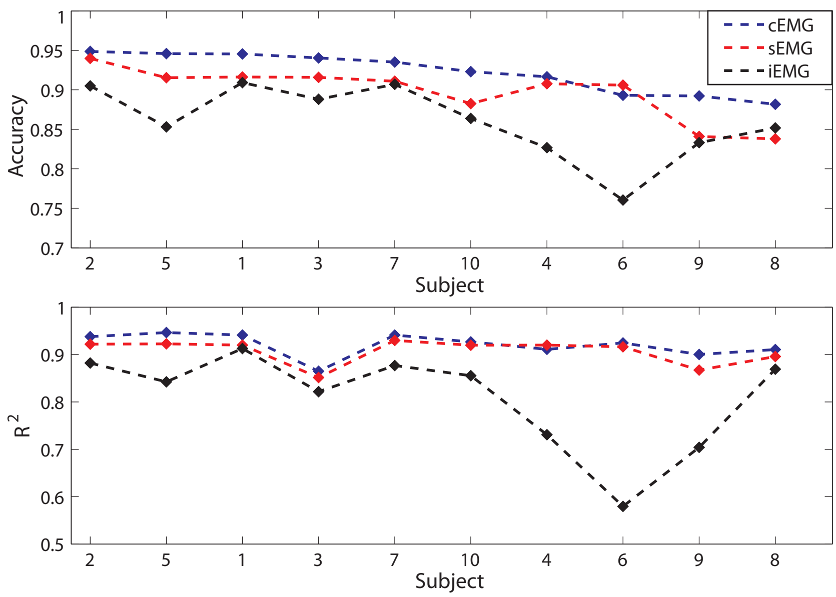

Figure 9.9: Classification accuracy and coefficient of determination (R^2) for each subject on the 9 class problem.

For the 9 class problem, a significant difference was found between all three signals ($p < 0.05$) for classification accuracy, where a mean accuracy of 92.2% ± 3.3 % was achieved with cEMG. For the remaining class combinations, sEMG and cEMG showed similar performance ($p > 0.05$) and generally both outperformed iEMG, see table 9.4. For classification accuracu, no general tendencies were found between the 3- and 5-class combinations, whereas the 9 class combination was significantly lower. No generel tendencies between class combinations for R^2 were found.

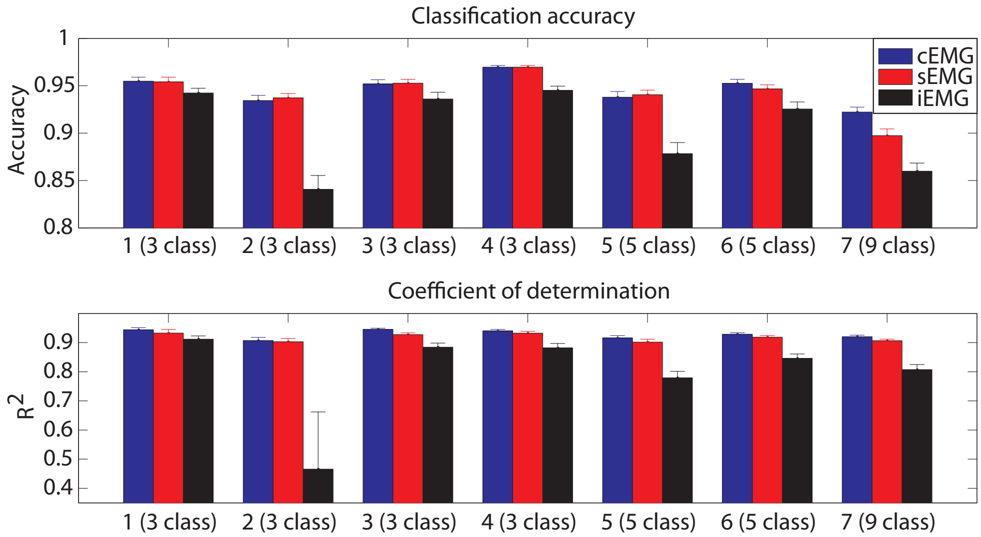

Figure 9.10: Classification accuracy and coefficient of determination (R^2) for several class combinations and all three signals. **1)** Flexion+extension. **2)** Pronation+Supination. **3)** Flexion/supination + extension/pronation. **4)** Flexion/pronation+supination/extension. **5)** Combination of classes 1) and 2). **6)** Combination of classes 3) and 4). **7)** Combination of classes 1), 2), 3) and 4). All includes rest as a class.

Modulated profile

When testing the control system on the modulated profile and training on trial one and two, a significant decrease in classification accuracy and R^2 was found compared to the four fold validation used in the previously described results ($p < 0.05$), see figure 9.11 and table 9.4. In general, sEMG and cEMG showed similar performance ($p > 0.05$) and generally both outperformed iEMG for classification accuracy and R^2, see table 9.4.

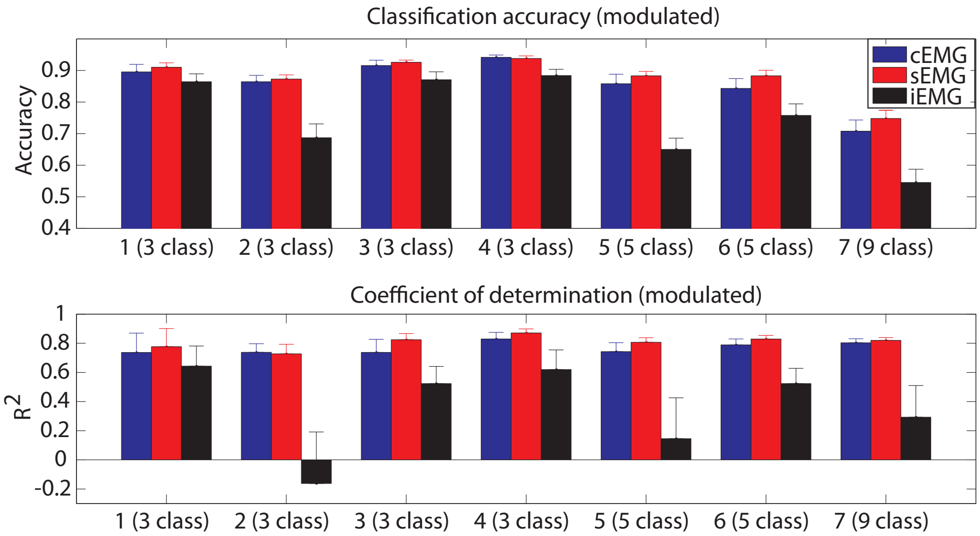

Figure 9.11: Classification accuracy and coefficient of determination (R^2) for several class combinations and all three signals for the modulated profile. **1)** Flexion+extension. **2)** Pronation+Supination. **3)** Flexion/supination + extension/pronation. **4)** Flexion/pronation+supination/extension. **5)** Combination of classes 1) and 2). **6)** Combination of classes 3) and 4). **7)** Combination of classes 1), 2), 3) and 4). All includes rest as a class.

Normal profile

	Acc [%]			R^2		
	cEMG	**sEMG**	**iEMG**	**cEMG**	**sEMG**	**iEMG**
1 (3 class)	$95.5 \pm 2.7^{*}$	$95.4 \pm 3.1^{\dagger}$	$94.2 \pm 3.2^{*/\dagger}$	$0.94 \pm 0.05^{*}$	$0.93 \pm 0.08^{\dagger}$	$0.91 \pm 0.07^{*/\dagger}$
2 (3 class)	$93.4 \pm 3.5^{*}$	$93.7 \pm 2.9^{\dagger}$	$84.1 \pm 9.2^{*/\dagger}$	$0.91 \pm 0.07^{*}$	$0.90 \pm 0.07^{\dagger}$	$0.47 \pm 1.24^{*/\dagger}$
3 (3 class)	95.2 ± 2.8	95.3 ± 2.6	93.6 ± 4.5	$0.95 \pm 0.02^{*/\dagger}$	$0.93 \pm 0.04^{*}$	$0.88 \pm 0.09^{\dagger}$
4 (3 class)	$97.0 \pm 1.2^{*}$	$97.0 \pm 1.1^{\dagger}$	$94.5 \pm 2.8^{*/\dagger}$	$0.94 \pm 0.03^{*}$	$0.93 \pm 0.04^{\dagger}$	$0.88 \pm 0.10^{*/\dagger}$
5 (5 class)	$93.8 \pm 3.8^{*}$	$94.1 \pm 3.1^{\dagger}$	$87.8 \pm 7.4^{*/\dagger}$	$0.92 \pm 0.05^{*}$	$0.90 \pm 0.07^{\dagger}$	$0.78 \pm 0.14^{*/\dagger}$
6 (5 class)	$95.3 \pm 2.7^{*}$	94.7 ± 2.8	$92.5 \pm 4.7^{*}$	$0.93 \pm 0.03^{*}$	$0.92 \pm 0.03^{\dagger}$	$0.85 \pm 0.09^{*/\dagger}$
7 (9 class)	$92.2 \pm 3.3^{*}$	$89.7 \pm 4.5^{*}$	$86.0 \pm 5.4^{*}$	$0.92 \pm 0.03^{*}$	$0.91 \pm 0.03^{*}$	$0.81 \pm 0.11^{*}$

Modulated profile

	Acc [%]			R^2		
	cEMG	**sEMG**	**iEMG**	**cEMG**	**sEMG**	**iEMG**
1 (3 class)	89.5 ± 7.5	91.0 ± 4.3	86.4 ± 7.9	$0.74 \pm 0.42^{*}$	$0.78 \pm 0.39^{\dagger}$	$0.64 \pm 0.44^{*/\dagger}$
2 (3 class)	$86.4 \pm 6.4^{*}$	$87.3 \pm 4.2^{\dagger}$	$68.7 \pm 13.9^{*/\dagger}$	0.74 ± 0.19	$0.73 \pm 0.21^{\dagger}$	$-0.16 \pm 1.12^{\dagger}$
3 (3 class)	$91.5 \pm 5.4^{*}$	$92.6 \pm 2.2^{\dagger}$	$87.1 \pm 7.9^{*/\dagger}$	0.74 ± 0.28	$0.82 \pm 0.14^{\dagger}$	$0.52 \pm 0.37^{\dagger}$
4 (3 class)	$94.2 \pm 2.2^{*}$	$93.8 \pm 2.6^{\dagger}$	$88.4 \pm 6.2^{*/\dagger}$	$0.83 \pm 0.14^{*}$	$0.87 \pm 0.09^{\dagger}$	$0.62 \pm 0.43^{*/\dagger}$
5 (5 class)	$85.8 \pm 9.5^{*}$	$88.3 \pm 4.4^{\dagger}$	$65.0 \pm 11.3^{*/\dagger}$	$0.74 \pm 0.19^{*}$	$0.81 \pm 0.10^{\dagger}$	$0.15 \pm 0.89^{*/\dagger}$
6 (5 class)	$84.3 \pm 9.9^{*}$	88.3 ± 5.5	$75.8 \pm 11.6^{*}$	$0.79 \pm 0.13^{*}$	$0.83 \pm 0.08^{\dagger}$	$0.52 \pm 0.33^{*/\dagger}$
7 (9 class)	$70.8 \pm 11.2^{*}$	$74.8 \pm 9.3^{\dagger}$	$54.5 \pm 13.3^{*/\dagger}$	$0.80 \pm 0.09^{*}$	$0.82 \pm 0.06^{\dagger}$	$0.29 \pm 0.69^{*/\dagger}$

Table 9.4: Classification accuracy and coefficient of determination (R^2) for several class combinations and all three signals. **1)** Flexion+extension. **2)** Pronation+Supination. **3)** Flexion/supination + extension/pronation. **4)** Flexion/pronation+supination/extension. **5)** Combination of classes 1) and 2). **6)** Combination of classes 3) and 4). **7)** Combination of classes 1), 2), 3) and 4). All includes rest as a class. A significant difference was found between the signals with matching symbols († and *) for that problem.

Investigation of mis-classifications

As seen on figure 9.12, the errors most frequently occur during transition between movements.

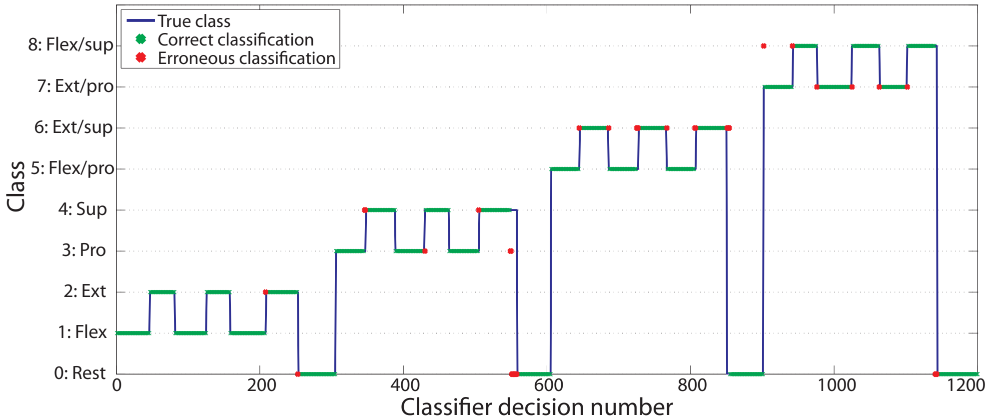

Figure 9.12: Representative example of the location of misclassification for subject 1 for a 9 class problem.

The effect of ignoring classifications around transitions from one class to another can be seen in figure 9.13 for the 9 class problem for the three signals. In general classification accuracy increased when an increasing number of classifications around the transitions were ignored; in particular when ignoring few outcomes.

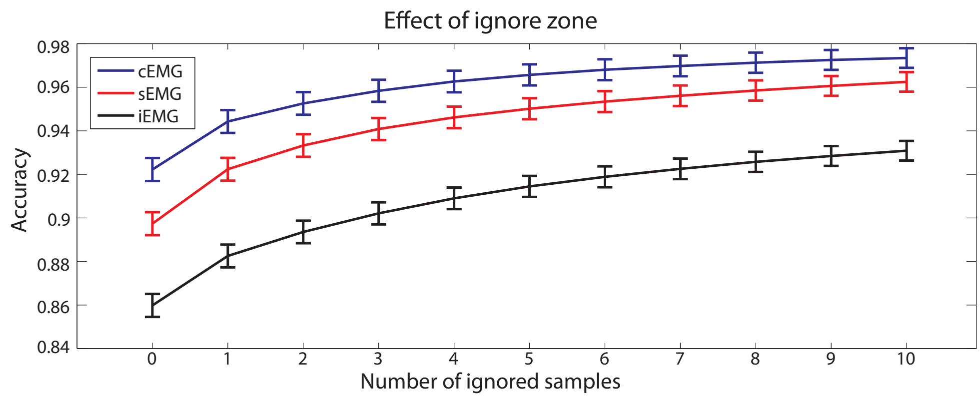

Figure 9.13: Effect on classification accuracy of ignoring outcomes around each transition for the complex 9-class problem.

The effect of the ignore zone on the different class combinations can be seen in figure 9.14 ignoring one and 5 outcomes, corresponding to 7.9 % and 38.3 % of the target force level.

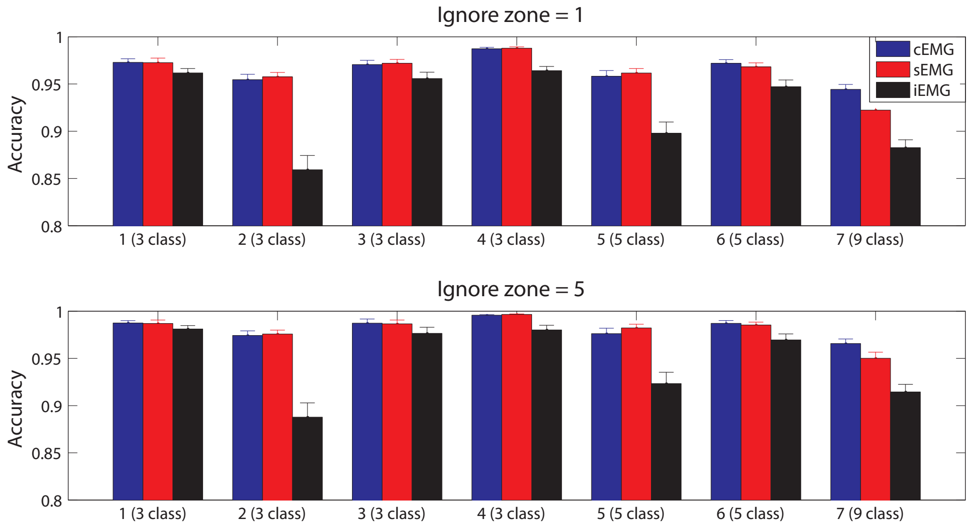

Figure 9.14: Classification accuracy and coefficient of determination (R^2) for several class combinations and all three signals with 1 and 5 values around each transition ignored. **1)** Flexion+extension. **2)** Pronation+Supination. **3)** Flexion/supination + extension/pronation. **4)** Flexion/pronation+supination/extension. **5)** Combination of classes 1) and 2). **6)** Combination of classes 3) and 4). **7)** Combination of classes 1), 2), 3) and 4). All includes rest as a class.

9.9 Summary of results

Throughout the results, the different parameters which impact the performance of the control scheme were investigated, and the system validated. The following describes the main findings:

- The significant highest classification accuracy for TD features was achieved using at least six features for cEMG and sEMG and at least four features for iEMG.
- The significant highest classification accuracy was found using features from the TD+TFD or the TD+FD+TFD.
- Filtering of the features increased classification accuracy significantly for LDA and kNN.
- The LDA classifier was significantly better than most other classifiers for both dimensionality reduction methods.
- Of the dimensionality reduction methods neither PCA or SEPCOR showed superior performance.
- Using MV did not show any significantly improved classification accuracies compared to a window of 400 ms.
- Neither of the investigated force estimators was significantly superior.
- For the nine class problem, a classification accuracy of 92.2 % for cEMG was achieved, which was significantly higher than both sEMG and iEMG.
- For the nine class problem, an R^2 of 0.92 for cEMG was achieved, which was significantly higher then both sEMG and iEMG.

- The modulated profile showed significantly worse performance compared to trial one and two.
- Most of the errors were located in shifts between movements. By ignoring 250 ms on either side of these shifts classification accuracy increased to 96.6 for the nine class problem using cEMG. %

Synthesis

III

Discussion 10

In this study, each step of the proposed myoelectric control system was investigated and optimized. The control system must allow precise control of sequential and simultaneous movements along with the corresponding force of two DoFs flexion/extension and pronation/supination of the wrist.

Feature domains

In the literature, feature extraction has received much attention in order to choose appropriate features. Phinyomark et al. investigated 37 features from the TD and FD for classification of six movements, where varying performance from using single features was found. Combining several features showed improved classification accuracy, which has also been shown in other studies. [Phinyomark et al., 2012; Oskoei and Hu, 2008]
Thus, to find the best feature set for the control system proposed in the current study, nine TD features were investigated in all possible combinations for each signal. In general, the classification accuracy increased with an increased number of used features up to eight. However, combining more than six features for sEMG and cEMG, and four features for iEMG did not significantly improve the accuracy, which is likely due to redundancy, as described by Phinyomark et al.. [Phinyomark et al., 2012]
The literature further suggests that using FD and TFD features may increase classification accuracy [Huang et al., 2005; Englehart et al., 2001]. In this work, it was found that adding features from the TFD or FD to the TD features significantly increased classification accuracy. Moreover, combining TD and TFD features was shown to outperform combining TD and FD features with an increase in classification accuracy of approximately 2.5 %. Englehart et al. showed that TFD features were good for especially the transient states of the EMG signal. This may explain the better TFD performance of the current work due to the dynamic nature of the acquired EMG signal and the frequent switches between movements [Englehart et al., 2001].

Filtering of features

Previously, extracted features have been filtered to remove spurious peaks in the feature space for both sEMG and iEMG. However, this has only been investigated for force estimation [Rosenvang et al., 2010b; Kamavuako et al., 2012]. In this work, the outcome of filtering the features was investigated for movement classification, where a significant increase in classification accuracy of up to 5 % was found for all signals for the kNN and LDA classifier. The positive effects may be due to a more consistent and localized grouping of classes in the feature space, which especially LDA and kNN classifiers require. [Duda et al., 2000]

Dimensionality reduction

Many studies perform dimensionality reduction on the feature space to avoid the curse of dimensionality when multiple features are used [Englehart et al., 1999; Hargrove et al., 2007, 2009]. PCA has previously been shown to be the superior dimensionality reduction method compared to class separability [Englehart et al., 1999]. However, other techniques based on PCA have shown better performance than the traditional PCA algorithm [Chu et al., 2006; Hargrove et al., 2009].
In the current study, another alternative technique called SEPCOR was investigated, which has been used previously in image processing [Ege et al., 2000]. The results showed that PCA achieved the overall highest accuracy with LDA, however, not significantly different from SEPCOR. Thus, based on the current results, SEPCOR could not be conclusively determined as inferior to PCA. On the contrary, SEPCOR showed a more consistent increase across all classifiers. Furthermore, increasing the explained variance for PCA in some cases led to a decrease in classification accuracy, whereas SEPCOR in all cases increased classification accuracy when increasing maximum allowed correlation.

Classifier

The choice of classifier has been investigated thoroughly in the literature [Scheme et al., 2011; Hargrove et al., 2007]. A study by Scheme et al. compared several classifiers (including the same classifiers as the current study) and found no significant differences between the investigated classifiers. This finding is further supported by Scheme and Englehart, arguing that the choice of features are more important than classifier. [Scheme et al., 2011; Scheme and Englehart, 2011]
The results from the current study showed that LDA had the overall best performance, however, only when including many variables. Otherwise the investigated classifiers had almost equal performance, which agrees well with the literature. The reason for the superior performance of LDA with at high number of variables may be due to the fact that the choice of features was based on the LDA classifier giving this particular classifier an advantage in the following optimization steps. Moreover, increasing the amount of dimensions in the feature space increases the possibility of classes being linearly separable.

Post-processing

Post-processing of the classified outcomes was performed through majority voting, given an acceptable delay of 200 ms. In this analysis, different window and step sizes was used. Majority voting was compared to a window of 400 ms inducing the same delay in the control system. The results revealed that majority voting did not increase

classification accuracy; on the contrary, for long step sizes majority voting resulted in significant decreased classification accuracy compared to the 400 ms window. Results from Englehart and Hudgins showed that when the window size increased, the accuracy from majority voting approached the accuracy from unprocessed decisions, i.e., less effect of using post-processing was found [Englehart and Hudgins, 2003]. This may explain why no difference was found with a window of 400 ms in the present study. Furthermore, it has previously been shown that a window of 160 ms with no majority voting provided better results than shorter windows with majority voting, taking both classification accuracy and computational efficiency into account [Farrell and Weir, 2008a].
However, it cannot be excluded that post-processing may be beneficial, if smaller steps were used, since this would provide more votes for the majority vote. A drawback of decreasing the step size is the increased computational demand on the processing unit, which increase the power consumption and thus drains the battery more quickly in a prosthesis.

Force estimator

For force estimation, the results showed no significant difference between the proposed force estimators (LM and ANN) for sEMG and iEMG. However, LM showed to be significantly better for cEMG. In the literature both linear and ANN based estimators have been used. Kamavuako et al. showed that grasping force could be estimated with high accuracy for iEMG using only one EMG channel and a single feature. These results were later extended to apply for sEMG by Bøg et al., investigating different single TD features. [Kamavuako et al., 2009; Bøg et al., 2011]
Nielsen et al. investigated the relationship between EMG and simultaneous wrist movements using an ANN and multiple features. Albeit the increased complexity, it was found that the ANN could precisely estimate the force of both movements [Nielsen et al., 2011]. In the present work, it was shown that the relationship between EMG and simultaneous movements could be explained equally well by a simple linear combination of the used variables, even though the complexity was the same as in Nielsen et al.. This may be due to the linearizing effects of the PCA and filtering of the features in the present study. [Kamavuako et al., 2012; Englehart et al., 1999]
These findings are supported by the simple case presented by Smidstrup et al., where no significant difference between the ANN and LM was found using single TD features linearly related to force. [Smidstrup et al., 2011]

Overall performance of the control system

When all parameters were found, the control system was validated on multiple class combinations. The highest classification accuracy for the nine class problem was 92.2 %, well above the reasonable expectations of a user, and an R^2 of 0.92 using cEMG [Scheme and Englehart, 2011]. As could be expected, fewer classes led to higher classification accuracies resembling results from other studies [Hargrove et al., 2009;

Farrell and Weir, 2008a].
Of notice is the three class problem pronation/supination and rest, which showed a degradation in classification accuracy for iEMG. This might be because the muscles pronator and supinator were not hit by the iEMG electrodes due to their relatively deep location. The same tendency was seen in the five-class problem including all single movements and rest.

EMG signal comparison

Generally, iEMG showed significantly lower classification accuracies than sEMG and cEMG for all class combinations. This was somewhat in contrast to a study Hargrove et al., where equal classification accuracies could be achieved for iEMG and sEMG in a 10 class problem. However, this study targeted specific muscles corresponding to the performed movements [Hargrove et al., 2007]. Another study by Farrell and Weir, comparing sEMG and iEMG using a targeted and untargeted technique, found no difference in classification accuracy between the four conditions when using both TD and AR features. However, a significant decrease in accuracy was found for untargeted iEMG using only TD features. The inconsistency between the results reported by Farrell and Weir and the current study may be due to the number of EMG channels used. Farrell and Weir used eight EMG channels and found that iEMG suffered more when using fewer channels than sEMG did, although only significant for one through three channels. As the proposed study only used six channels and a more complex task, this may contribute to the significant difference between sEMG and iEMG. Most importantly, in this work dynamic movements with frequent shifts were investigated, which are much more complex in nature compared to steady-state contractions as used by Farrell and Weir. [Farrell and Weir, 2008a]
With respect to R^2 no other studies have used an untargeted technique for proportional control, and further no studies have investigated iEMG for simultaneous movements. The results of the proposed control system for iEMG showed a similar tendency for R^2 as for movement classification (lower accuracy for iEMG). Albeit using an untargeted technique, the obtained R^2 from sEMG and cEMG (0.91 and 0.92 respectively) compared well with a study by Nielsen et al., where specific muscles were targeted (R^2 0.93). [Nielsen et al., 2011]

In general, cEMG outperformed sEMG and iEMG. This could be explained by the different information content encoded in sEMG and iEMG. Thus, for complex problems, e.g. simultaneous movements, sEMG and iEMG may complement each other rather than being alternatives.

Generality of the control system

To assess the generality of the control system, it was tested on a modulated profile with varying amplitude and frequency. It was found that validating on the modulated profile showed significant decrease in both classification accuracy and R^2. This implies that the system was not general enough to support movements performed differently from the training of the system. This is a general weakness of pattern recognition based methods, where changes in the pattern degrade the performance, which may be overcome by adaptive EMG pattern recognition systems. [Scheme and Englehart, 2011]

Dynamic movements and transients

Since the experiment was composed of dynamic movements with frequent shifts, the entire data set could be regarded as semi-transient with transient shifts. In earlier studies, transient data has been shown to be particularly difficult to classify. [Englehart et al., 2001; Oskoei and Hu, 2007]
In the present study, the influence of transitions on classification was investigated by applying an ignore zone. The outcome confirmed that indeed most errors occurred in the transitions, since classification accuracy increased from 92.2 % to 97.3 % ignoring 10 outputs (corresponding to 500 ms) for the nine class problem using the cEMG signal. In general across all class combinations, an improvement in classification accuracy was achieved by ignoring both one and five outcomes on either side of each transition.
This approach of eliminating transitions is by no means new, as it has been used by different authors to improve classification accuracy and allow comparison to classification on steady state data. Huang et al., Oskoei and Hu and Chan and Englehart removed 256 ms on either side of a transition equivalent to approximately five outcomes in the proposed control system. Doing so, classification accuracies of up to 96.6 % could be achieved for the nine class problem, and as high as 98.7 % for a five class problem using cEMG.
In this work, force could be precisely estimated and thus, in the future, this could be used to classify to rest at low forces potentially achieving accuracies similar to the above.

Methodological aspects

Throughout the experiment, several issues became clear. The position of the intramuscular electrodes might shift during the experiment causing a slight change in the pick-up area and thus the measured EMG signal. Although all signals were observed during recording, a slight change would not be observed. Consequently, the pattern of even the same movement would differ making it difficult to be recognized by the classifier. When inserting the intramuscular electrodes, verification of the location was done based on observed activity during various wrist and hand movements. However, to ensure a muscle was hit, a stimulator could be used to induce muscle twitch.
Especially the simultaneous torque profiles posed a challenge for some subjects, which may cause them to perform non-reproducible movements. The used torque levels were empirically verified as a comfortable low to medium level for males and

females. However, especially for combined movements, this was not true across all subjects, where some subjects expressed a high level of effort to reach the target force level whilst others found it very easy. This may be due to the design of the dynamometer, where the size and positioning of the hand was found to influence how much force was needed. In these cases, the subjects may be prune to fatigue of the muscles, which changes the measured muscle pattern.

Even though the proportional control scheme was used to estimate the produced torque, the output can also be used to estimate the velocity of a movement proportional to the used torque. [Englehart et al., 2001]
This can be used to develop a multi-functional prosthesis, where large EMG activity can be interpreted to either move the prosthetic hand in a certain direction quickly or with a large amount of force, if resistance towards the movement is perceived.

Practical aspects

In the current study, healthy subjects were used for data acquisition. However, it may be questioned whether the obtained results can be generalized for amputees. In a study by Scheme et al., EMG signals from both healthy and amputee subjects were collected using untargeted recording sites on the forearm. Here it was shown that pattern recognition based classifiers show a decrease in performance for transradial amputees compared to healthy subjects. However, it was shown that the same relative performance of the features and classifiers were found for healthy and amputees. This indicates that finding the optimal system based on healthy individuals, as in the current work, can also be expected to perform optimally for amputees albeit with lower accuracy. [Scheme and Englehart, 2011]

When considering the used features in the optimal control system, adding TFD features imposes increased computational load. Thus, in the future, it might be interesting to investigate the performance of the proposed control system only with TD features. Moreover, it was found that LDA was the optimal for movement classification, and that LM and ANN showed equal performance for force estimation. This is important, since LDA and LM were the fastest among the investigated classifiers and force estimators. This is encouraging when considering the real-time prospects of the proposed control system.

Conclusion 11

In this study we investigated how control of a myoelectric prosthesis could be improved for transradial amputees by allowing precise control of dynamic, simultaneous movements with corresponding force estimation. Such an improvement would allow movements of a prosthetic device to be more fluent and less robot like. Throughout the analysis, it was investigated how this could be achieved, and it was found that a hybrid between a pattern recognition based control scheme for movement classification, and a proportional control scheme for force estimation should be developed. The hybrid control scheme was based on both sEMG and iEMG and supported wrist flexion/extension and wrist pronation/supination.

To develop such a system, an experiment was conducted including 10 healthy individuals using untargeted recording sites. To gain optimal control, the parameters influencing performance of the control system were thoroughly investigated and optimized.

This control system allowed classification of nine classes of motion comprising rest and control of single and simultaneous DoFs with a mean accuracy above 92 %. Removing transients between movements, this result could be increased to above 97 % comparable to studies with movements of less complexity. The control system also allowed precise estimation of the corresponding force with a mean R^2 of 0.92 across all subjects. Thus, we have shown that the novel approach of using a hybrid control scheme can be succesfully implemented to allow intuitive control of dynamic, simultaneous DoFs with high accuracy.
Although further studies are needed, these results are very promising for final control of a myoelectric prosthesis. Furthermore, the optimal system was composed of relatively simple processing techniques computationally, and thus has a large potential for real time control of a myoelectric prosthesis.

12 List of abbreviations

The present chapter includes a list of all abbreviations used trough out this report. The abbreviations are listed in an alphabetic order.

- ANN: Artificial neural network
- AR: Autoregressive
- cEMG: Combined sEMG and iEMG
- CoM: Center of mass
- CNS: Central nervous system
- CSE: Constraint sample entropy
- DoF(s): Degree(s) of Freedom
- DWTMAV: Discrete wavelet transform, mean absolute value
- DWTRMS: Discrete wavelet transform, root mean square
- EMG: Electromyography
- FD: Frequency domain
- FR: Frequency ratio
- GMM: Gaussian mixture model
- HMM: Hidden Markov model
- iEMG: Intramuscular electromyography
- kNN: k nearest neighbor
- LDA: Linear discriminant analysis
- LM: Linear model
- MAV: Mean absolute value
- MAVSLP: Mean absolute value slope
- MDF: Median frequency
- MNF: Mean frequency
- MU: Motor unit
- MVC: Maximum voluntary contraction
- PCA: Principal component analysis
- PSD: Power spectral density
- R^2: Coefficient of determination
- RMS: Root mean square
- sEMG: Surface electromyography
- SEPCOR: Separability and correlation
- SN: Signal noise difference
- SSC: Slope sign changes
- STFT: Short time Fourier transform
- SVMOAA: Support vector machine, one against all
- SVMOAO: Support vector machine, one against one
- TD: Time domain

- TFD: Time frequency domain
- VAR: Variance
- WL: Waveform length
- WT: Wavelet transform
- WPT: Wavelet packet transform
- MV: Majority vote
- MSV: Mean square value
- WAMP: Willison amplitude
- ZC: Zero crossings
- QoL: Quality of Life

Bibliography

Abe, **2010**. Shigeo Abe. *Support Vector Machines for Pattern Classification*. Springer, 2010.

Ajiboye and Weir, **2005**. Abidemi Bolu Ajiboye and Richard F. Weir. *A Heuristic Fuzzy Logic Approach to EMG Pattern Recognition for Multifunctional Prosthesis Control*. IEEE Transactions on neural systems and rehabilitation engineering, 13(3), 280–291, 2005.

Battye, Nightengale, and Whillis, **1955**. C. K. Battye, A. Nightengale, and J. Whillis. *The use of myo-electric current in the operation of prostheses*. The Journal og Bone and Joint Surgery, 37, 506–510, 1955.

Beale, Hagan, and Demuth, **2012**. Mark Hudson Beale, Martin T. Hagan, and Howard B. Demuth. *Neural Network Toolbox^{TM} 7 - User's Guide*. The MathWorks, Inc, 7th edition, 2012.

Bøg, Erkocevic, Niemeier, Mathiesen, Smidstrup, , and Kamavuako, **2011**. M.F. Bøg, E. Erkocevic, M.J. Niemeier, J.R. Mathiesen, A. Smidstrup, , and E.N. Kamavuako. *Investigation of the Linear Relationship between Grasping Force and Features of Intramuscular EMG*. 15th NBC on Biomedical Engineering & Medical Physics, IFMBE Proceedings, 34, 121–124, 2011.

Bottomley, **1965**. A. H. Bottomley. *Myo-electric Control of Powered Prostheses*. The Journal og Bone and Joint Surgery, 47, 411–415, 1965.

Chan and Englehart, **2005**. Adrian D. C. Chan and Kevin B. Englehart. *Continuous Myoelectric Control for Powered Prostheses Using Hidden Markov Models*. IEEE Transactions on Biomedical Engineering, 52, 121–124, 2005.

Chu, Moon, and Mun, **2006**. Jun-Uk Chu, Inhyuk Moon, and Mu-Seong Mun. *A Real-Time EMG Pattern Recognition System Based on Linear-Nonlinear Feature Projection for a Multifunction Myoelectric Hand*. IEEE Transactions on Biomedical Engineering, 53, 2232–2239, 2006.

Corder and Foreman, **2009**. Gregory W. Corder and Dale I. Foreman. *Nonparametric Statistics for Non-Statisticians*. John Wiley & Sons, inc., 2009.

Cotton, Cranny, Chappell, White, and Beeby, **2007**. D.P.J. Cotton, A. Cranny, P.H. Chappell, N.M. White, and S.P. Beeby. *Control Strategies for a Multitiple* *degree of Freedom Prosthetic Hand*. The Journal of the Institute of Measurement and Control, 40, 24–27, 2007.

d'Avella, Portone, Fernandez, and Lacquaniti, **2006**. Andrea d'Avella, Alessandro Portone, Laure Fernandez, and Francesco Lacquaniti. *Control of Fast-Reaching Movements by Muscle Synergy Combinations*. The Journal of Neuroscience, 30, 7791–7810, 2006.

Dorcas and Scott, **1966**. D. S. Dorcas and R. N. Scott. *A Three-State Myo-electric Control*. Med. & biol. Engng., 4, 367–370., 1966.

Duda, Hart, and Stork, **2000**. Richard O. Duda, Peter E. Hart, and David G. Stork. *Pattern Classification*. Wiley-Interscience, 2nd edition, 2000. ISBN-13: 978-0-471-05669-0.

Ege, Hejlesen, Larsen, Møller, Jennings, Kerr, and Cavan, **2000**. Bernhard M. Ege, Ole K. Hejlesen, Ole V. Larsen, Karina Møller, Barry Jennings, David Kerr, and David A. Cavan. *Screening for diabetic retinopathy using computer based image analysis and statistical classification*. Computer Methods and Programs in Biomedicine, 62, 165–175, 2000.

Englehart, Hudgins, Parker, and Stevenson, **1999**. K. Englehart, B. Hudgins, P.A. Parker, and M. Stevenson. *Classification of the myoelectric signal using time-frequency based representations*. Medical Engineering & Physics, 21, 431–438, 1999.

Englehart and Hudgins, **July 2003**. Kevin Englehart and Bernard Hudgins. *A robust, real-time control scheme for multifunction myoelectric control*. IEEE Transactions on Biomedical Engineering, 50(7), 848–854, 2003.

Englehart, Hudgins, and Parker, **2001**. Kevin Englehart, Bernard Hudgins, and Philip A. Parker. *A Wavelet-Based Continuous Classification Scheme for Multifunction Myoelectric Control*. IEEE Transactions on Biomedical Engineering, 48, 302–311, 2001.

Epstein, Heinemann, and McFarland, **2010**. Richard A. Epstein, Allen W. Heinemann, and Lynne V. McFarland. *Quality of life for veterans and servicemembers with major traumatic limb loss from Vietnam and OIF/OEF conflicts*. JRRD, 47(4), 373–386, 2010.

Esquenazi, **2004**. Alberto Esquenazi. *Amputation rehabilitation and prosthetic restoration. From surgery to community reintegration*. Disability and Rehabilitation, 26(14/15), 831–836, 2004.

Farina, Leclerc, Arendt-Nielsen, Buttelli, and Madeleine, **2008**. Dario Farina, Frédéric Leclerc, Lars Arendt-Nielsen, Olivier Buttelli, and Pascal Madeleine. *The change in spatial distribution of upper trapezius muscle activity is correlated to contraction duration*. Journal of Electromyography and Kinesiology, 18, 16–25, 2008.

Farrell and Weir, **2008a**. Todd R. Farrell and Richard F. Weir. *A Comparison of the Effects of Electrode Implantation and Targeting on Pattern Classification Accuracy for Prosthesis Control*. IEEE Transactions on biomedical engineering, 55(9), 2198–2211, 2008.

Farrell and Weir, **2008b**. Todd R. Farrell and Richard F. Weir. *Analysis Window Induced Controller Delay for Multifunctional Prostheses*. MEC '08 Measuring Success in Upper Limb Prosthetics, 1, 13–15, 2008.

Hargrove, Englehart, and Hudgins, **2007**. Levi J. Hargrove, Kevin Englehart, and Bernard Hudgins. *A Comparison of Surface and Intramuscular Myoelectric Signal Classification*. IEEE Transactions on Biomedical Engineering, 54(5), 847–853, 2007.

Hargrove, Li, Englehart, and Hudgins, **2009**. Levi J. Hargrove, Guanglin Li, Kevin B. Englehart, and Bernard S. Hudgins. *Principal Components Analysis Preprocessing for Improved Classification Accuracies in Pattern-Recognition-Based Myoelectric Control*. IEEE Transactions on biomedical engineering, 56(5), 1407–1414, 2009.

Hargrove, Scheme, Englehart, and Hudgins, **2010**. Levi J. Hargrove, Erik J. Scheme, Kevin B. Englehart, and Bernard S. Hudgins. *Multiple Binary Classifications via Linear Discriminant Analysis for Improved Controllability of a Powered Prosthesis*. IEEE Transactions on Neural Systems and Rehabilitation Engineering, 18, 49–57, 2010.

Hoozemans and Dieën, **2005**. Marco J.M. Hoozemans and Jaap H. van Dieën. *Prediction of handgrip forces using surface EMG of forearm muscles*. Journal of electromyography and kinesiology, 15, 358–366, 2005.

Huang, Englehart, Hudgins, and Chan, **2005**. Yonghong Huang, Kevin B. Englehart, Bernard Hudgins, and Adrian D. C. Chan. *A Gaussian Mixture Model Based Classification Scheme for Myoelectric Control of Powered Upper Limb Prostheses*. IEEE Transactions on Biomedical Engineering, 52, 1801–1811, 2005.

Jiang, **2009**. Ning Jiang. *Extracting Simultaneous and Proportional Neural Control Information for Multiple-DOF Prostheses From the Surface Electromyographic Signal*. Transactions on Biomedical Engineering IEEE, 56, 1070–1080, 2009.

Jones and Lederman, **2006**. Lynette A. Jones and Susan J. Lederman. *Human Hand Function*. Oxford University Press, 1st edition, 2006. ISBN-13: 978-0-19-517315-4.

Kamavuako, Farina, Yoshida, and Jensen, **2009**. Ernest Nlandu Kamavuako, Dario Farina, Ken Yoshida, and Winnie Jensen. *Relationship between grasping force and features of single-channel intramuscular EMG signals*. Journal of Neuroscience Methods, 185, 143–150, 2009.

Kamavuako, Rosenvang, Bøg, Smidstrup, Erkocevic, Niemeier, Jensen, and Farina, 2012. Ernest Nlandu Kamavuako, Jakob Celander Rosenvang, Mette Frydensbjerg Bøg, Anne Smidstrup, Ema Erkocevic, Marko Jörg Niemeier, Winnie Jensen, and Dario Farina. *Influence of the feature space on the estimation of hand grasping force from intramuscular EMG*. IN PRESS, 2012.

Brian M. Kelly, Percival H. Pangilinan Jr., Gianna M. Rodriguez, Robert C. Mipro, and Valerie S. Bodeau, 2011. Brian M. Kelly, Percival H. Pangilinan Jr., Gianna M. Rodriguez, Robert C. Mipro, and Valerie S. Bodeau. *Upper Limb Prosthetics*. Medscape, 2011.

Kendall, McCreary, Provance, Rodgers, and Romani, 2005. Florence Peterson Kendall, Elizabeth Kendall McCreary, Particia Geise Provance, Mary McIntyre Rodgers, and Wiliam Anthony Romani. *Muscles - Testing and Function with Posture and Pain*. Lippincott Williams & Wilkins, 5th edition, 2005.

Khezri and Jahed, 2007. Mahdi Khezri and Mehran Jahed. *Real-time intelligent pattern recognition algorithm for surface EMG signals*. BioMedical Engineering OnLine, 6, 1–12, 2007.

Komi and Tesch, 1979. Paavo V. Komi and Per Tesch. *EMG Frequency Spectrum, Muscle Structure, and Fatigue During Dynamic Contractions in Man*. Eur. J. Appl. Physiol., 42, 41–50, 1979.

Luca and Erim, 1994. Carlo J. De Luca and Zeynep Erim. *Common drive of motor units in regulation of muscle force*. Trends in Neurosciences, 17, 299–305, 1994.

Martini, 2006. Frederic H. Martini. *Funfamentals of Anatomy and Physiology*. Pearson, 7th edition, 2006. ISBN-13: 978-0805372809.

Mathworks, 2012. Mathworks. *Statistics Toolbox*. Mathworks, 2012.

Merletti and Parker, 2004. Roberto Merletti and Philip Parker. *Electromyography - Physiology, Engineering, and Noninvasive Applications*. John Wiley & Sons, inc., 2004.

Miguelez, Conyers, Lang, and Gulick, 2010. John Miguelez, Dan Conyers, MacJulian Lang, and Kristin Gulick. *Upper Exteimity Prosthetics*. Office of Surgeon General, 2010.

Nielsen, Holmgaard, Jiang, Englehart, Farina*, and Parker, 2011. Johnny L. G. Nielsen, Steffen Holmgaard, Ning Jiang, Kevin B. Englehart, Dario Farina*, and Phil A. Parker. *Simultaneous and Proportional Force Estimation for Multifunction Myoelectric Prostheses Using Mirrored Bilateral Training*. IEEE Transactions on biomedical engineering, 58(3), 681–688, 2011.

Onishi, Yagi, Akasaka, Momose, Ihashi, and Handa, 2000. H. Onishi, R. Yagi, K. Akasaka, K. Momose, K. Ihashi, and Y. Handa. *Relationship between EMG signals and force in human vastus lateralis muscle using multiple bipolar wire electrodes*. Journal of Electromyography and Kinesiology, 10, 59–67, 2000.

Oskoei and Hu, **2008**. Mohammadreza Asghari Oskoei and Huosheng Hu. *Support Vector Machine-Based Classification Scheme for Myoelectric Control Applied to Upper Limb*. IEEE Transactions on Biomedical Engineering, 55, 1956–1965, 2008.

Oskoei and Hu, **2006**. Mohammadreza Asghari Oskoei and Huosheng Hu. *GA-based Feature Subset Selection for Myoelectric Classification*. International Conference on Robotics and Biomimetics, 2006.

Oskoei and Hu, **2007**. Mohammadreza Asghari Oskoei and Huosheng Hu. *Myoelectric control systems—A survey*. Biomedical Signal Processing and Control, 2, 275–294, 2007.

Paciga, Richard, and Scott, **1980**. J. E. Paciga, P.D. Richard, and R.N. Scott. *Error rate in five-state myoelectric control systems*. Med. & Biol. Eng. & Comput, 18, 287–290, 1980.

Parker, Englehart, and Hudgins, **2006**. P. Parker, K. Englehart, and B. Hudgins. *Myoelectric signal processing for control of powered limb prostheses*. Journal of Electromyography and Kinesiology, 18, 541–584, 2006.

Phinyomark, Hirunviriya, Limsakul, and Phukpattaranont, **2010**. A. Phinyomark, S. Hirunviriya, C. Limsakul, and P. Phukpattaranont. *Evaluation of EMG feature extraction for hand movement recognition based on euclidean distance and standard deviation*. Electrical Engineering/Electronics Computer Telecommunications and Information Technology (ECTI-CON), International Conference, 1, 856 – 860, 2010.

Phinyomark, Limsakul, and Phukpattaranont, **2011**. A. Phinyomark, C. Limsakul, and P. Phukpattaranont. *Application of Wavelet Analysis in EMG Feature Extraction for Pattern Classification*. Measurement Science Review, 11, 45–52, 2011.

Phinyomark, Phukpattaranont, and Limsakul, **2012**. Angkoon Phinyomark, Pornchai Phukpattaranont, and Chusak Limsakul. *Feature reduction and selection for EMG signal classification*. Expert Systems with Applications, 39, 7420–7431, 2012.

Rosenvang, Bøg, Erkocevic, Niemeier, Smidstrup, and Kamavuako, **2010a**. Jakob C. Rosenvang, Mette F. Bøg, Ema Erkocevic, Marko J. Niemeier, Anne Smidstrup, and Ernest N. Kamavuako. *Prediction of grasping force based on features of surface and intramuscular EMG*. 2010.

Rosenvang, Bøg, Erkocevic, Niemeier, Smidstrup, and Kamavuako, **2010b**. Jakob Celander Rosenvang, Mette F. Bøg, Ema Erkocevic, Marko J. Niemeier, Anne Smidstrup, and Ernest N. Kamavuako. *Prediction of grasping force based on features of surface and intramuscular EMG*. UNPUBLISHED, 2010.

Scheme and Englehart, **2011**. Erik Scheme and Kevin Englehart. *Electromyogram pattern recognition for control of powered upper-limb prostheses: State of the art and challenges for clinical use*. Journal of Rehabilitation Research & Development, 48, 643–660, 2011.

Scheme, Englehart, and Hudgins, **2011**. Erik J. Scheme, Kevin B. Englehart, and Bernard S. Hudgins. *Selective Classification for Improved Robustness of Myoelectric Control Under Nonideal Conditions*. IEEE Transactions on Biomedical Engineering, 58, 1698–1705, 2011.

Scott, **1967**. R. N. Scott. *Myoelectric Control of Prostheses and Orthoses*. Bulletin of Prosthetics Research, pages 93–114, 1967.

Silbernagl and Despopoulos, **2009**. Stefan Silbernagl and Agamemno Despopoulos. *Color atlas of physiology*. Thieme, 6th edition, 2009.

Smidstrup, Erkocevic, Niemeier, Bøg, Rosenvang, and Kamavuako, **2011**. A. Smidstrup, E. Erkocevic, M.J. Niemeier, M.F. Bøg, J.C. Rosenvang, and E.N. Kamavuako. *A Comparison Study of EMG Features for Force Prediction*. 15th NBC on Biomedical Engineering & Medical Physics, IFMBE Proceedings, 1, 93–96, 2011.

Winkler, **2009**. Sandra L. Hubbard Winkler. *Upper limb amputation and prosthetics epidemiology, evidence, and outcomes*. Textbooks of Military Medicine, Care of the Combat Amputee, 2009.

Zar, **2010**. Jerrold H. Zar. *Biostatistical analysis*. Pearson Educational International, 5th edition, 2010.

Zecca, Micera, Carrozza, and Dario, **2002**. M. Zecca, S. Micera, M. C. Carrozza, and P. Dario. *Control of multifunctional prosthetic hands by processing the electromyographic signal*. Biomedical Engineering, 30(4-6), 459 – 485, 2002.